PREPARATION AND APPLICATION OF $ZnFe_2O_3/\alpha\text{-}Al_2O_3$ COMPOSITE PHOTOCATALYSTS FOR TEXTILE EFFLUENT TREATMENT

BY

Alhaji Saleh ZANNA UMARA

DEPARTMENT OF CHEMICAL ENGINEERING

AHMADU BELLO UNIVERSITY

ZARIA – NIGERIA

FEBRUARY, 2016



PREPARATION AND APPLICATION OF $ZnFe_2O_3/\alpha\text{-}Al_2O_3$ COMPOSITE PHOTOCATALYSTS FOR TEXTILE EFFLUENT TREATMENT

BY

Alhaji Saleh ZANNA UMARA (B. ENG.UNIMAID) 2010

MSc/ENG/20682/2012-2013

A DISSERTATION SUBMITTED TO THE SCHOOL OF POSTGRADUATE STUDIES, AHMADU BELLO UNIVERSITY, ZARIA

IN PARTIAL FULFILLMENT OF THE REQUIREMENTS FOR THE AWARD OF A MASTER OF SCIENCE DEGREE IN CHEMICAL ENGINEERING

DEPARTMENT OF CHEMICAL ENGINEERING

AHMADU BELLO UNIVERSITY, ZARIA

NIGERIA

FEBUARY, 2016

DECLARATION

I declare that the work in this dissertation entitled "preparation and application of $ZnFe_2O_3/\alpha$-Al_2O_3 composite photocatalysts for textile effluent treatment" has been carried out by me in the Department of Chemical Engineering Ahmadu Bello University, Zaria. The information derived from the literature has been duly acknowledged in the text and list of references provided. No part of this dissertation was previously presented for another degree or diploma at this or any other Institution.

ZANNA UMARA Alhaji Saleh _____ _____

Signature Date

CERTIFICATION

This dissertation entitled "preparation and application of $ZnFe_2O_3/\alpha\text{-}Al_2O_3$ composite photocatalysts for textile effluent treatment" by Alhaji Saleh ZANNA UMARA meets the regulations governing the award of Master of Science in Chemical Engineering of the Ahmadu Bello University, Zaria and is approved for its contribution to knowledge and literacy presentation.

Dr. Abdulhamid Hamza	_____	_____
Chairman Supervisory Committee	Signature	Date
Dr. Diya' uddeen B.H.	_____	_____
Member Supervisory Committee	Signature	Date
Dr. S. M. Waziri	_____	_____
Head, Department of Chemical Engineering, A.B.U. Zaria	Signature	Date
Professor Kabir Bala	_____	_____
Dean, postgraduate School, A.B.U. Zaria	Signature	Date

ACKNOWLEDGEMENT

This dissertation is the outcome of numerous hours involving arduous research and the culmination of a process that included the constant assistance, support and guidance afforded to me by teaching and non-teaching staff members of the Department of Chemical Engineering, A.B.U, Zaria. This achievement been accomplished, in no small measure, due to their sheer professionalism and dedication which they demonstrated on several occasions.

I hold in high esteem my able teacher and supervisor Engr. Dr. Abdulhamid Hamza. All through this work he has been of astute and invaluable help. He has been able to skilfully manage this research without forgetting the ever essential human relationships. I would like to appreciate my able minor supervisor, so also my Boss Engr. Dr. Diya' uddeen B.H., for his unique intellectual guidance. My sincere gratitude goes to my role modelEngr. Prof. I.M.Bugaje, for being an outstanding guardian, advisor and excellent contributor to the success of this achievement. My sincere appreciation goes to Engr. Dr. Abdul aziz Atta, Mal. Abbas and BK M. Aji for thier wonderful assistace to the success of this work.

A special mention to my parents (ALHAJI ZANNA UMARA and LATE HAJJA HAFSAT ALH.SALEH) who through thick and thin were always there for me and never doubted my abilities to achieve my goal. Thanks for your constant support and enthusiasm.

I would like to use this medium to thank my friends and colleagues especially Dr. Tasiu, Jajere, Mahamud, Abdul, Jamilu, Tobba, Ahmad, Sani, Bugaje, Mas'ud, Habibu, Muktar, Antony, Benga, Abdulrauf, Iron Laddy, Kate, Ango, Ahmad, Salisu and my brothers and Sisters who enabled me to seamlessly continue my dissertation.

All these thanks are, however, only a fraction of what is due to the Almighty (ALLAH) for granting me an opportunity and the strength to successfully accomplish this assignment. You are the greatest and Powerful.

ABSTRACT

Photocatalysis has continued to attract increasing attention due to its numerous applications in the energy and environmental fields. Present work was aimed at the development of $ZnFe_2O_4$ and α-Al_2O_3 supported $ZnFe_2O_4$ visible – light responsive photocatalysts for the treatment of textile effluent. $ZnFe_2O_4$ and α-Al_2O_3 supported $ZnFe_2O_4$ were synthesized using co–precipitation route followed by calcination at 500 ^{0}C. The synthesized photocatalysts were characterized using x–ray diffraction (XRD), Specific surface area analysis, Scanning electron microscopy (SEM) and pH at point of zero charge analysis (pH_{pzc}), respectively. XRD analysis revealed low crystallinity of the synthesized $ZnFe_2O_4$. The specific surface areas of the photocatalysts decrease with increase in the $ZnFe_2O_4$ loadingon the surface of the support. SEM analysis showed that the size of $ZnFe_2O_4$ particles is much smaller than that of the α-Al_2O_3support, and that $ZnFe_2O_4$ are uniformly dispersed on the supports. The pH_{pzc} was found to increase with increase in the $ZnFe_2O_4$. The photocatalytic activity of the synthesized photocatalysts was evaluated by studying the decolourization kinetics of methylene blue (MB).The $ZnFe_2O_4$ is characterized by low crystallinity. The size of $ZnFe_2O_4$ particles is smaller than that of the α-Al_2O_3 support. The percentage degradation of MB increased with increase in the $ZnFe_2O_4$ loading from 10 wt% to 30 wt% and decreased when the loading was raised to 40 wt%. The photocatalytic activity of 30 wt % $ZnFe_2O_4$/α-Al_2O_3 is higher than those of $ZnFe_2O_4$ and other α-Al_2O_3 supported photocatalysts containing 10 wt%, 20 wt% and 40 wt% of $ZnFe_2O_4$. α-Al_2O_3 support improves the photocatalytic activity of $ZnFe_2O_4$ under visible light irradiation, and the optimum loading of $ZnFe_2O_4$ on α-Al_2O_3 is 30 wt %. Analysis of the kinetic data for the photocatalytic degradation of MB using the Langmuir–Hinshelwood kinetic model yielded 0.005 $mgL^{-1}min^{-1}$ for the intrinsic photocatalytic reaction rate constant and 0.111 Lmg^{-1} for the adsorption equilibrium constant. Photocatalytic treatment of real textile effluent resulted in more effective (when compared to photolytic treatment) in the reduction of effluent's colour, COD, pH, conductivity and TDS. 30 wt% $ZnFe_2O_4$/Al_2O_3 was found to be more effective than bare $ZnFe_2O_4$ for the reduction of effluent's colour, COD, pH, conductivity and TDS.

TABLE OF CONTENT

Cover Page i

Title Page ii

DECLARATION iii

CERTIFICATION iv

ACKNOWLEDGEMENT v

ABSTRACT vi

TABLE OF CONTENT vii

LIST OF ABBREVIATIONS xii

CHAPTER ONE 1

INTRODUCTION 1

1.1 General background of the study 1

1.2 PROBLEM STATEMENT 2

1.3 AIM AND OBJECTIVES 3

1.4 SCOPE 3

1.5 JUSTIFICATION 4

CHAPTER TWO 5

LITERATURE REVIEW 5

2.1 Textile effluent 5

2.1.1 Environmental Impacts of Textile Effluent 9

2.2 Conventional Methods for Treating Textile Effluents 15

2.2.1 Primary treatment methods of textile effluents 15

2.2.1 Secondary method of treating textile effluents 17

2.2.3 Tertiary methods of treating textile effluent 18

2.3 Photocatalysis 20

2.4 Zinc ferrite and its composites as photocatalysts. 24

2.5 Synthesis of ferrites 26

2.5.1 Thermal methods 27

2.5.2 Sol–gel and citrate methods 28

2.5.3 Co-precipitation methods 28

2.5.4 Solid-state reactions 28

2.6 Visible Light Photocatalysis 29
2.7 Applications of photocatalytic processes 30
2.8 Kinetics of photocatalytic processes 32
2.9 Characterization of solid photocatalysts 36
2.9.1 Surface area analysis using sear's method. 36
2.9.2 Crystal phase structure analysis. 36
2.9.3 Surface morphology analysis. 37
2.10 Methylene blue (MB) 38
2.11 α-Alumina 42
2.12 Some Previous Related Works 42
CHAPTER THREE 44
3.1 The following is the list of materials and equipment used in this work. All chemicals listed were obtained from Stevemore chemical store in Zaria, Nigeria. 44
3.2 Materials and equipment 44
3.2 Methods 46
3.2.1 Synthesis of $ZnFe_2O_4$ and $ZnFe_2O_4/Al_2O_3$ 47
3.3 Characterization of the synthesized $ZnFe_2O_4$ and $ZnFe_2O_4/\alpha\text{-}Al_2O_3$ composites. 47
3.4.1 X-Ray Diffraction (XRD) Spectroscopy 47
3.4.2 SEM Analysis 48
3.4.3 Specific surface area determination 48
3.4.4 Determination of the pH of point of zero charge 48
3.5 Photocatalytic experiments 49
3.5.1 Photocatalytic decolorization of MB solution 49
3.5.1 Photocatalytic degradation of MB solution 50
3.6 Analysis of the raw and treated water samples 50
3.6.1 UV- Visible spectroscopic analysis 50
3.6.2 Measurement of COD 50
3.6.3 Measurement of pH 51
3.6.4 Measurement of Conductivity 51
3.6.5 Measurement of TDS 51
CHAPTER FOUR 52
RESULTS AND DISCUSSION 52

4.1. Characterization of the synthesized photocatalysts 52
4.1.1 XRD analysis of the synthesized Photocatalysts 52
4.1.2. Specific Surface Areas of the Synthesized Photocatalysts 55
4.1.3 Morphology of the synthesized photocatalyst 55
4.1.4. pH at zero of point charge of the photocatalyst 56
4.2. Photocatalytic decolourization of MB using the synthesized photocatalyst 57
4.3 Photocatalytic treatment of textile effluent 61
4.4.1. Photocatalytic decolourization of textile effluent 62
4.4.2 Photocatalytic degradation of textile effluent 63
CHAPTER FIVE 65
CONCLUSIONS AND RECOMMENDATIONS 65
5.1 Conclusions 65
5.2 Recommendations 66
REFERENCES 67
APPENDIX A 81
Material balance 81
$ZnCl_2 + 2FeCl_2 + 8NaOH \rightarrow Zn(OH)_2 + 2Fe(OH)_3 + 8NaCl$ (1) 81
APPENDIX B 83
CRYSTALLITE SIZE ANALYSIS USING XRD 83
APPENDIX C 87
SURFACE AREA DETERMINATION 87
APPENDIX D 88
DETERMINATION OF POINT OF ZERO CHARGE OF THE SYNTHESIZED CATALYSTS 88
APPENDIX E 91
UV-vis ANALYSIS OF DECOLOURIZED MB SOLUTION 91
APPENDIX F 92
DETERMINATION OF COD OF DEGRADED MB SOLUTION 92

List of Table

Table 2.1. Types of textile wastes produced 6

Table 2.2. Average water consumptions for various fabrics 8

Table 2.3. Water required by cotton textile industry for the wet process 8

Table 2.4. Water required by synthetic textile industry for its wet process 9

Table 2.5. Characteristics of typical untreated textile wastewater 11

Table 2.6. Typical concentration of unfixed dyes in textile effluents 13

Table 2.7. Discharge limits of industrial effluents in some countries 14

Table 2.8. Redox potential for oxidizing agents in water 24

Table 2.9. Applications of Photocatalysis 31

Table 3.1. List of equipment used and their specifications 45

Table 4.1. Average particle sizes and specific surface areas of the synthesized $ZnFe_2O_4$ and α-Al_2O_3 supported $ZnFe_2O_4$ 55

Table 4.2. pH at point of zero charge of the photocatalysts 57

Table 4.3. Properties of the raw and treated textile effluent 62

List of Figures

Fig. 2.1. Band gaps of selected photocatalysts. Casbbeer et al.,(2011). 21

Fig. 2.2. Proposed mechanism of Photocatalysis. Hoffmann *et al.*, (1995); Peralta-Hernández et al., (2007) 22

Fig. 2.3. Preparation methods of ferrites using Fe(III) and M(II) salts as precursors. Zhang *et al*., (2011) 27

Fig. 2.4. The solar spectrum (ASTM: **www.astm.org**) 30

Fig. 2.5. Typical XRD pattern of ZnFe2O4 Prithviraj Swamy *et al*., (2010). 37

Fig. 2.6. (b) SEM image of $ZnFe_2O_4$ reported by Jadhav *et al*., (2010) and (c) TEM image of $ZnFe_2O_4$ reported by Chen *et al*., (2010) 38

Fig. 2.7. Structure of MB, Disanto *et al*., (1972) 39

Fig. 3.1. Flow Diagram of the Research Methodology 46

Fig. 4.2: SEM image of (a) Pure $ZnFe_2O_4$ and (b) $ZnFe_2O_4/\alpha\text{-}Al_2O_3$ composite. 56

Fig. 4.3. Photocatalytic degradation of MB using $ZnFe_2O_4$ and $\alpha\text{-}Al_2O_3$ supported Z_2nFeO_4..... 59

Fig. 4.4 Effect of initial concentration of MB on its photocatalytic degradation using 30 wt % $ZnFe_2O_4/\alpha\text{-}Al_2O_3$ 60

Fig. 4.5 Langmuir–Hinshelwood kinetic plot for the photocatalytic degradation of MB using 30 wt % $ZnFe_2O_4/\alpha\text{-}Al_2O_3$ 61

Fig. 4.6 Decolourization of textile effluent via photolysis and photocatalysis using $ZnFe_2O_4$ and 30 wt% $ZnFe_2O_4/\alpha\text{-}Al_2O_3$. [Irradiation time - 90 mins. photocatalyst dose - 0.1 g/L] 63

Fig. 4.7. COD removal from textile effluent via photolysis and photocatalysis using ZnFe2O4 and 30 wt% $ZnFe_2O_4/\alpha\text{-}Al_2O_3$. [Irradiation time - 90 mins. photocatalyst dose - 0.1 g/L] 64

LIST OF ABBREVIATIONS

AOPs	Advance Oxidation Processes
BET	Brunaur – Emmett – Teller
BOD	Biological Oxygen Demand
CB	Conduction Band
COD	Chemical Oxygen Demand
CPC	Compound Parameter Collector
EEM	Electrical Energy per Mass
EEO	Electrical Energy per Order
FT	Flat Tube
rGO	Graphene Oxide
JCPDS	Joint Committee on Powder Diffraction Standard
L – H	Langmuir – Hinshelwood
MB	Methylene Blue
MWCNT	Molecular Weight Carbon Nano Tube
NTO	Nano Tube Oxidation
ROS	Reactive Oxidant Spacies
SC	Semiconductor
SEM	Scanning Electron Microscope
TDS	Total Dissolve Solid
UV	Ultraviolet
VB	Valence Band

CHAPTER ONE

INTRODUCTION

1.1 General background of the study

Water pollution due to the release of chemicals from industrial sectors has been a major concern in recent times. The major constituents of industrial effluents are heavy metals, pesticides, dyes, aliphatic and aromatic compounds, detergents, chlorophenols, etc. Many conventional methods (such as sedmentation, chlorination, precipitation, etc) are used to treat these effluents and each method has its own advantages and shortcomings (Nagaveni *et al.*, 2005). Recently, advanced oxidation processes (AOPs), especially photocatalysis, have become techniques for wastewater treatment, because they convert organic contaminants to a large extent into stable less toxic compounds, such as carbon dioxide and water. The high reactivity of hydroxyl radical generated by the AOPs plays an important role in oxidizing the organic species present in wastewater into harmless species (Hameed*et al.*, 2009). Heterogeneous photocatalysis by semiconductor materials, such as TiO_2, ZnO, Fe_2O_3, CdS, GaP, and ZnS has indeed been widely used for the degradation of various organic and inorganic pollutants (Faber*et al.*, 2005).

Photocatalysts are important materials that provide a relatively simple means for the conversion of light energy including (solar energy) for use in oxidation and reduction process. They utilize light energy (*hν*) to carry out oxidation and reduction reactions. When irradiated with light energy, an electron (e^-) is excited from the valence band (VB) to the conduction band (CB) of photocatalysts, leaving a photogenerated hole (h^+). The produced e^- and h^+ enable oxidation and reduction processes to occur. Whenphotocatalytic process takes place in aqueous solutions, water and hydroxide ions react with photogenerated h^+ to form hydroxyl radicals ($^*OH$) which is the primary oxidant in the photocatalytic oxidation of organic compounds (Cao*et al.*, 2007).

Zinc ferrite ($ZnFe_2O_4$) has been applied as a visible light responsive photocatalyst for the remediation of hazardous wastes, contaminated groundwater and control of toxic air contaminants (Jadhav*et al.*, 2010). To enhance the photocatalytic activity of $ZnFe_2O_4$, several methods have been proposed for its synthesis with unique size dependent physical and chemical properties. Various composites of $ZnFe_2O_4$ ($ZnFe_2O_4/TiO_2$, $ZnFe_2O_4$/ZnO etc) have also been synthesized and their photocatalytic activity is often higher than that of the bare $ZnFe_2O_4$ (Cao*et al.*, 2007).

In this work,$ZnFe_2O_4$ and $ZnFe_2O_4/\alpha\text{-}Al_2O_3$ have been synthesized via co-precipitation route, and characterized using XRD, SEM, pH_{zpc} and specific surface area analyses. The photocatalytic activity of the synthesized materials was evaluated by studying the kinetics of photocatalytic decolourization of methylene blue (MB) under visible light irradiation using a 500 W halogen lamp. $ZnFe_2O_4$ and the best $\alpha\text{-}Al_2O_3$supported $ZnFe_2O_4$ were then applied for the degradation of real textile effluent.

1.2 PROBLEM STATEMENT

a. Separation of photocatalyst particles after wastewater treatment limits large scale application of photocatalysis.

b. Photocatalytic activity of $ZnFe_2O_4$ is relatively low due to fast recombination of photogenerated electron-hole pairs.

c. Preparation and photocatalytic properties of $ZnFe_2O_4/\alpha\text{-}Al_2O_3$ composites have not been reported in the literature (to the best of my knowledge).

1.3 AIM AND OBJECTIVES

The aim of this project was to synthesize and characterize $ZnFe_2O_4$ and $ZnFe_2O_4/\alpha\text{-}Al_2O_3$ composite photocatalysts with varying $ZnFe_2O_4$ to $\alpha\text{-}Al_2O_3$ ratio and apply them for the treatment of textile effluent.

The specific objectives were:

a. Synthesis of $ZnFe_2O_4$ and $ZnFe_2O_4/\alpha\text{-}Al_2O_3$ composites in various proportions using co-precipitation method.

b. Characterization of the synthesized materials using XRD, SEM, Specific surface area and pH_{pzc} analysis.

c. Evaluation of the photocatalytic activity of the materials using decolourization of methylene blue(MB) as a model reaction.

d. Application of $ZnFe_2O_4$ and the best $ZnFe_2O_4/\alpha\text{-}Al_2O_3$composite for the photocatalytic degradation of model anionic and cationic dyes.

e. Application of $ZnFe_2O_4$ and the best $ZnFe_2O_4/\alpha\text{-}Al_2O_3$for the photocatalytic treatment of real textile effluent.

1.4 SCOPE

This work involves synthesis of $ZnFe_2O_4$and $ZnFe_2O_4/\alpha\text{-}Al_2O_3$ composites in various ratios (with 10 wt%; 20 wt%: 30 wt%; and 40 wt% $ZnFe_2O_4$), characterization and application of the synthesized composites for degradation of MBand textile effluent under visible light illumination.

1.5 JUSTIFICATION

a. Photocatalysis has promising applications in energy generation and environmental remediation.

b. $ZnFe_2O_4/\alpha\text{-}Al_2O_3$ composites are easy to synthesize.

c. $ZnFe_2O_4/\alpha\text{-}Al_2O_3$ composites may be used to degrade various organic compounds under solar and/or visible light irradiation.

d. The amount of energy needed in photocatalytic technology is low.

e. The photocatalysts can be easily separated after use because of the magnetic property of $ZnFe_2O_4$.

CHAPTER TWO

LITERATURE REVIEW

2.1 Textile effluent

The textile industry is considered to be one of the biggest threats to the environment. The various processes carried out in the textile industries produce large amounts of gaseous, liquid and solid wastes (Muostafa, 2008). Some of the most commonly generated wastes are listed in Table 2.1. The textile industry uses a variety of chemicals and a large amount of water for its manufacturing steps. Water is mainly used for: (a) the application of chemical onto textiles and (b) rinsing the manufactured textiles (Ntuli *et al*., 2009). The amount of water consumed by various types of fabrics is listed in Table 2.2. However, the exact quantity of water required varies from industry to industry depending on the dyeing process and the type of fabrics produced. About 80-150 $m^3$of water are used to produce 1 kg of fabrics. It was also estimated that about 1,000-3,000 $m^3$of wastewater is reproduced after processing about 12-20 tonnes of textiles per day (Atif, 2002). The amount of water consumed by cotton and synthetic textile producing industries are shown in Tables 2.3 and 2.4.

The water let out after the production of textiles contains a large amount of dyes and other chemicals which are harmful to the environment. The level of toxicity or harmfulness of the textile effluents varies among industries (Kiriakidou *et al*., 1999). In the textile dyeing process, there is always a portion of unfixed dye which gets washed away along with water. The textile wastewater is found to be high (Georgiou *et al*., 2003).

Table 2.1. Types of textile wastes produced

Process	Emission	Wastewater	Solid Wastes
Fibre preparation	Little or none	Little or none	Fibre waste and packaging waste
Yarn spinning	Little or none	Little or none	Packaging wastes, sized yarn, fibre waste, cleaning and processing waste
Slashing/sizing	VOCs	BOD, COD, metals, cleaning waste, size	Fibre lint, yarn waste, packaging waste, unused starch-based sizes
Weaving	Little or none	Little or none	Packaging waste yarn and fabric scraps, off - spec fabric, used oil
Knitting	Little or none	Little or none	Packaging waste, yarn, fabric scraps.
Desizing	VOCs from glycol esters	BOD from sizes lubricants, biocides, anti-static compounds	Packaging waste, fibre lint, yarn waste, cleaning and maintenance materials
Bleaching	Little or none	H_2O_2, stabilizers, high pH	Little or none
Dyeing	VOCs	Metals, salt, surfactants,organic processing assistants, cationic materials, colour, BOD, COD, sulphide,	Little or none

		acidity/alkalinity, spent solvents	
Printing	Solvents, acetic acid-drying and curing oven emission combustion gases	Suspended solids, urea, solvents, colour, metals, heat, BOD, foam	Little or none
Finishing	VOCs, contaminants in purchased chemicals, formaldehyde vapours, combustion gases	COD, suspended solids, toxic materials, spent solvents	Fabric scraps and trimmings, packaging waste

Source: Moustafa, (2008).

Table 2.2. Average water consumptions for various fabrics

Processing Subcategory	Water Consumption (m^3/ ton fibre material)		
	Minimum	Median	Maximum
Wool	111	285	659
Woven	5	114	508
Knit	2	84	377
Carpet	8.3	47	163
Stock/yarn	3.3	100	558
Nonwoven	2.5	40	83

Source: Moustafa, (2008).

Table 2.3. Water required by cotton textile industry for the wet process

Process	Water Consumption (L/1000 kg of products)
Sizing	500 - 8200
Desizing	2500 – 21000
Scouring	20000 – 45000
Bleaching	25000 – 25000
Mercerizing	17000 – 32000
Dyeing	10000 – 30000
Printing	8000 - 16000

Source: (Ntuli *et al*., 2009).

Table 2.4. Water required by synthetic textile industry for its wet process

Process	Water Requirements (L/1000 kg of products)				
	Rayon	Acetate	Nylon	Acrylic/Modacrylic	Polyester
Scouring	17000 - 34000	25000 – 84000	50000 – 67000	50000 - 67000	50000 - 67000
Salt bath	4000 - 12000	-	-	-	-
Bleaching	-	33000 – 50000	-	-	-
Dyeing	17000 - 34000	34000 – 50000	17000 – 34000	17000 - 34000	17000 – 34000
Special finishing	4000 - 12000	24000 – 12000	32000 – 48000	40000 - 56000	8000 - 12000

Source: (Ntuli*et al*., 2009).

2.1.1 Environmental Impacts of Textile Effluent

Human exposures to textile dyes have resulted in lung and skin irritations, headaches, congenital malformations and nausea (Lima *et al*., 2007). Detected benzidine, a known carcinogen in a textile effluent which contained disperse orange 37, disperse blue 373 and disperse violet 93 dyes. (Marcucci*et al*., 2002) tested a total of seven dyes (cremazoles blue S1, cremazoles brown GR, cremazoles orange 3R, direct bordeaux, direct royal blue, direct congo red and direct violet) using AMES tests and witnessed the presence of mutagenic agents. It was noted that direct violet was the only dye with a mutagenicity ratio less than 2:0. They observed that the cremazoles dyes were so toxic to microorganisms (Morikawa*et al*., 1997), reported evidence of kidney, liver and urinary bladder cancers on workers after prolonged exposure to textile dyes. It was found that

dermatitis, asthma, nasal problems and rhinitis were acquired by workers after prolonged exposure to reactive dyes (Nilsson *et al*., 1993).

The characteristics of textile effluents vary and depend on the type of textile manufactured and the chemicals used. The textile wastewater effluent contains high amounts of agents causing damage to the environment and human health including suspended and dissolved solids, biological oxygen demand (BOD), chemical oxygen demand (COD), chemicals, odour and colour. Most of the BOD/COD ratios are found to be around 1:4, indicating the presence of non-biodegradable substances (Arya*et al*., 2009). Typical characteristics of textile effluent are shown in Table 2.5

Table 2.5. Characteristics of typical untreated textile wastewater

Parameter	Range
pH	6-10
Temperature (°C)	35-45
Total dissolved solids (mg/L)	8,000-12,000
BOD (mg/L)	80-6,000
COD (mg/L)	150-12,000
Total suspended solids (mg/L)	15-8,000
Total Dissolved Solids (mg/L)	2,900-3,100
Chlorine (mg/L)	1,000-6,000
Free chlorine (mg/L)	<10
Sodium (mg/L)	10
Trace elements (mg/L)	**Range**
Fe	<10
Zn	<10
Cu	<10
As	<10
Ni	<10
B	<10
F	<10
Oil & grease (mg/L)	10-30

Table 2.5. Characteristics of typical untreated textile wastewater continued

TNK (mg/L)	10-30
NO_3-N (mg/L)	<5
Free ammonia (mg/L)	<10
SO_4 (mg/L)	600-1000
Silica (mg/L)	<15
Total Kjeldahl Nitrogen (mg/L)	70-80
Color (Pt-Co)	50-2,500

Source: Moustafa, (2008)

Textile effluents contain trace metals like Cr, As, Cu and Zn, which are capable of harming the environment (Eswaramoorthi *et al*., 2008). Dyes in water give out a bad colour and can cause diseases like haemorrhage, ulceration of skin, nausea, severe irritation of skin and dermatitis (Nese*et al*., 2007). They can block the penetration of sunlight from water surface preventing photosynthesis (Laxman, 2009). Dyes also increase the biochemical oxygen demand of the receiving water and in turn reduce the reoxygenation process and hence hamper the growth of photoautotrophic organisms (Nese*et al*., 2007). The suspended solid concentrations in the effluents play an important role in affecting the environment as they combine with oily concentration of these unfixed dyes. The majority of the processes being carried out in textile industries produce gaseous emissions. Boilers, ovens and storage tanks are the three most important sources of air pollution in the textile industry. The boilers generate sulphur oxides and nitrogen. The high temperature textile drying process emits hydrocarbons. Pollutants are also emitted from residues of fibre preparation during the heat settling process. Gases can also be

emitted from chemicals during the dyeing process.The concentration of these unfixed dyes are as shown in Table 2.6.

Table 2.6. Typical concentration of unfixed dyes in textile effluents

Fibre	Dye Type	Unfixed Dye (mg/L)
Wool and nylon	Acid dyes/reactive dyes for wool	7-20
	Pre-metallised dyes	2-7
	Azoic dyes	5-10
	Reactive dyes	20-50
Cotton and viscose	Direct dyes	5-20
	Pigment	1
	Vatdyes	5-20
	Sulphur dyes	30-40
Polyester	Disperse	8-20
Acrylic	Modified basic	2-3

Source: Rong *et al*., 2012).

The seriousness of water pollution depends on the quantity of water and chemicals used in the wet process (Laxman, 2009). Dye concentration in a dye house range from 0.01g/L to 0.25 g/L depending on the type of the environment and pollution caused by the textile industry. Some countries imposed certain limits on the disposal of effluents into the environment. Some of

theseregulations imposed are presented in Table 2.7. The disposal limits are found to differ from country to country. However, a constant check is to be kept on these discharge limits every now and then to maintain a safe and a healthy environment (Yusuffand Sonibare, 2004).

Table 2.7. Discharge limits of industrial effluents in some countries

Parameter	China	BIS	Thailand	Indonesia	Bangladesh	Nigeria
pH	6-9	5.5-9	5-9	6-9	6.5-9	6.0-9.0
Temperature (^{0}C)	-	50	-	-	40-45	-
Colour (Pt-Co)	80	None	-	-	-	None
TDS (mg/L)	-	2100	2000-5000	-	2100	2000 mg/L
TSS (mg/L)	150	100	30-150	60	100	30 mg/L
Sulphide (µg/L)	1000	2000	-	-	1000	-
Free Chlorine (µg/L)	-	1000	-	-	-	-
COD (mg/L)	200	250	120-400	250	200	50 mg/L
BOD5 (mg/L)	60	30	20-60	85	150	-
Oil & Grease (mg/L)	-	10	300	5	10	-
Dissolved Oxygen (µg/L)	-	-	-	-	4500-8000	-
Chromium (µg/L)	-	100	500	500	2000	-
Aluminium (µg/L)	-	-	-	-	-	
Copper (mg/L)	1000	1000	1000	2000	500	

Source: Doe (2008)

2.2 Conventional Methodsfor Treating Textile Effluents

Effluents discharged from the textile industries undergo various physico-chemical treatments such as flocculation, coagulation and ozonation and biological treatment for the removal of nitrogen, organics, phosphorus and metal removal (Adinand Asanto, 1996).

The disadvantages of the physico-chemical treatment processes are:

(i) The formation and disposal of sludge and

(ii) The required space.

The disadvantage of biological treatment processes are:

(i) The presence of toxic heavy metals in the effluent which affects the growth of microorganism

(ii) Most of the dyes used are a non-biodegradable in nature and

(iii) The long time required for treating the effluent

Generally, treatment of textile effluents involves three treatment processes: primary, secondary and tertiary treatments (Eswaramoothi *et al*., 2008).

2.2.1 Primary treatment methods of textile effluents

The first step in textile wastewater treatment is the removal of suspended solids, excessive quantities of oil and grease and gritty materials (Eswaramoothi*et al*., 2008). The effluent is first screened for coarse suspended materials such as yarns, lint, pieces of fabrics, fibres and rags using bar (Barclay and Buckley, 2000). Several environmental protection agencies worldwide have imposed rules entrusted with the protection of human health and guidelines for diminishing risk associated to the environment (Daneshvar *et al.*,2007).The screened effluent then undergoes settling for the removal of the suspended particles. The floating particles are removed by

mechanical scraping systems. Neutralization is done to reduce the acidic contents of the effluents. Sulphuric acid and boiler flue gas are the most commonly used chemicals to alter the pH. A pH value of 5-9 is considered ideal for the treatment process (Babu *et al*., 2007).

The first step of screening (coarse screening), the effluent is carried out to prevent damages from plastics, metals paper and rags. Coarse screens have an opening of 6 mm or larger. Coarse screening is followed by fine screening (1.5-6 mm opening) and very fine screening (0.2- 1.5mm opening). Fine screening helps in the reduction of suspended solids in the effluent. Screening is followed by sedimentation which makes use of gravity to settle the suspended particles such as clay or silts present in the effluent. According to Daneshvar*et al*., (2007), simple sedimentation was not found to be effective because it does not remove colloidal particles in the effluents. Another disadvantage of the process is the large space it occupies. Therefore, settling could be carried out by coagulation. Colloidal particles in the effluent carry charges on their surfaces and addition of chemicals to the effluent changes the surface property of the colloids hence causing them to clump together and settle. Ferrous sulphate, lime, alum, ferric sulphate and ferric chloride are some of the most commonly used chemicals in the coagulation step (Chen*et al*., 1996). The settled particles are collected as sludge. Disposal of sludge is one of the biggest challenges of treatment plants (Aryaand Kohli, 2009).

Mechanical flocculation is a physical process which involves slow mixing of the effluent with paddles bringing the small particles together to form heavier particles that can be settled and removed as sludge (Tripathy and De, 2006). One of the disadvantages with flocculation system is, Difficulty of control of floc formation.

2.2.1 Secondary method of treating textile effluents

The Secondary treatment process is mainly carried out to reduce the BOD, phenol and oil contents in the wastewater and to control its colour. This can be biologically done with the help of microorganisms under aerobic or anaerobic conditions. Aerobic Bacteria use organic matter as a source of energy and nutrients. They oxidize dissolved organic matter to $CO_2$and water and degrade nitrogenous organic matter into ammonia. Aerated lagoons, trickling filter and activated sludge systems are among the aerobic system used in the secondary treatment. Anaerobic treatment is mainly used to stabilize the generated sludge (Daneshvar *et al.*,2007).

Aerated lagoons are one of the commonly used biological treatment processes. This consists of a large holding tank lined with rubber or polythene and the effluent from the primary treatment is aerated for about 2-6 days and the formed sludge is removed. The BOD removal efficiency is up to 99% and the phosphorous removal is 15-25% (Daneshvar *et al.*, 2007). The nitrification of ammonia is also found to occur in aerated lagoons. Additional TSS removal can be achieved by the presence of algae in the lagoon (EPA, 2002). The major disadvantage of this technique is the large amount of space it occupies and the risk of bacterial contamination in the lagoons (Lafond, 2008).

Trickling filters are another common method of secondary treatment that mostly operates under aerobic conditions. The effluent for the primary treatment is trickled or sprayed over the filter. The filter usually consists of a rectangular or circular bed of coal, gravel, Poly Vinyl Chloride (PVC), broken stones or synthetic resins (Etter *et al*., 2011). A gelatinous film, made up of microorganisms, is formed on the surface of the filter medium. These organisms help in the oxidation of organic matter in the effluent to carbon dioxide and water (NODPR, 1995). Trickling filters do not require a huge space, hence making them advantageous compared to

aerated lagoons. However, their disadvantage is the high capital cost and odour emission (Etter *et al*., 2011). Aerobic activated sludge processes are commonly used. It involves a regular aeration of the effluent inside a tank allowing the aerobic bacteria to metabolize the soluble and suspended organic matters. A part of the organic matter is oxidized into $CO_2$and the rest are synthesized into new microbial cells (NESC, 2003). The effluent and the sludge generated from this process are separated using sedimentation; some of the sludge is returned to the tank as a source of microbes. A BOD removal efficiency of 90-95% can be achieved from this process, but is time consuming (Yasui*et al.*, 1996).

Sludge's formed as a result of primary and secondary treatment processes pose a major disposal problem. They cause environmental problems when released untreated as they consist of microbes and organic substances (Wainwright and Crossley, 2013).

2.2.3 Tertiary methods of treating textile effluent

There are several technologies used in tertiary treatments including electrodialysis, reverse osmosis and ion exchange. Electrolytic precipitation of textile effluents is the process of passing electric current through the textile effluent using electrodes. As a result of electro chemical reactions, the dissolved metal ions combine with finely dispersed particles in the solution, forming heavier metal ions that precipitate and can be removed later (Karos, 2013). One of the disadvantages is that a high contact time is required between the cathode and the effluent (Daneshvar *et al.,* 2007).

Reverse osmosis is a well-known technique which makes use of membranes that have the ability to remove total dissolved solid contents along with ions and larger species from the effluents. A high efficiency of > 90% has been reported (Babu*et al.,* 2007). Cotton dyeing processes use

electrolytes such as NaCl in high concentrations. These high concentrations of salts can be treated using reverse osmosis membrane (Kannan*et al*., 2006).

Electrodialysis is another process which uses membranes, that has the ability to separate dissolved salts. The electricity used in electrodialysis influences the ions to get transported through a semi permeable membrane by passing an electrical potential across water (WTS, 2012). The membranes used are charge specific and anion-selective which allows negatively charged particles to pass through and traps positively charged particles and vice versa. Placing numerous membranes throughout the system hinders the flow of effluent and the effluent would reach a point at which the ions are trapped or settled down and the remaining ions are neutral in charge (Jurenka, 2010). Membrane fouling (the process where solutes or other particles get attached to the membrane or into the membrane pore) has to be prevented by removing suspended solids, colloids and turbidity prior to electrodialysis (Marcucci,*et al*., 2002).

Ion exchange method is a commonly used tertiary method which involves the passage of effluents through the beds of ion exchange resins. These ion exchange resins are either cationic or anionic charged. Effluent passing through a cationic resin would have its cations removed by the resin and replaced with hydrogen ions making it acidic. When the acid solution is passed through anion resin, the anions would be substituted with hydroxyl ions (WWS, 2013).

Photocatalytic degradation is another tertiary method by which a wide range of dyes can be degraded depending on their molecular structures (Vautier, 2001). Adsorption is also found to be effective in the removal of colours. Thermal evaporation using sodium persulfate is also found to have a good oxidizing potential. This process is found to be eco-friendly because they do not have the property to form sludge and also do not emit toxic chlorine fumes during evaporation (Daneshvar *et al.,*2007).The presence of air and aerobic bacteria which convert the sludge into

carbon dioxide biomass and water. Anaerobic treatment involves the absence of air and the presence of anaerobic bacteria, which degrade the sludge into biomass, methane and carbon dioxide (Mittal, 2011).

2.3 Photocatalysis

In recent times considerable attention has focused on the safety and efficiency of water treatment technologies (Hrudey, 2009). Conventional water treatment processes such as ozonolysis and chlorination create disinfection by-products (DBP) such as bromate and trihalomethanes respectively, which have health risks (Hamidin *et al.*, 2008; Hrudey, 2009). In order to avoid such problems, attention is now being focused on Advance Oxidation Processes (AOPs) such as photocatalysis and Fenton oxidation.

Photodegradation is defined by the International Union of Pure and Applied Chemistry (IUPAC) as "*the photochemical transformation of a molecule into lower molecular weight fragments, usually in an oxidation process*" (Venkatachalam*et al.*, 2007). This process is usually too slow and inefficient to be useful in water treatment and requires the addition of a photocatalyst. These catalysts are activated by light and the resulting photocatalytic reactions are defined by IUPAC as "*catalytic reaction involving light absorption by a catalyst or by a substrate*" (Von Gunten and Hoigne, 1994).

Semiconductors are used as photocatalysts, because they have a narrow band gap between the valence and conduction bands suitable for the absorption of visible and UV light which is shown on Fig. 2.1. In order for photocatalysis to proceed, semiconductors need to absorb energy equal to or more than its energy gap to generate electron – hole pairs.

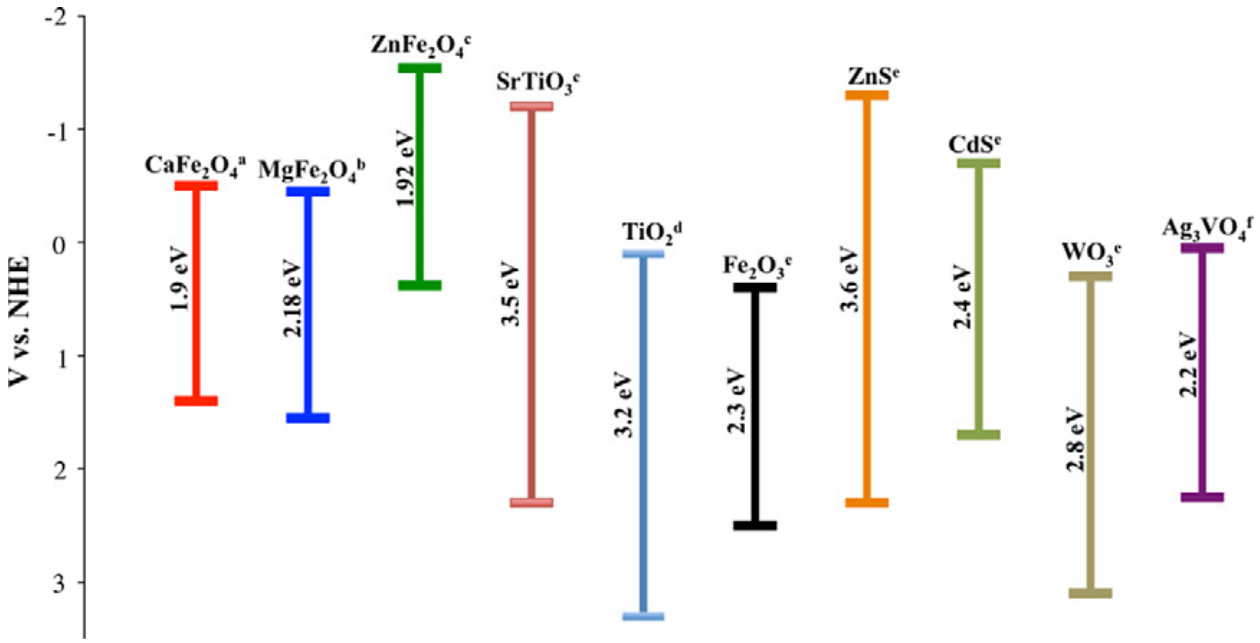


Fig. 2.1. Band gaps of selected photocatalysts. Casbbeer et al.,(2011).

The general mechanism of heterogeneous photocatalysis is illustrated in Fig. 2.2 for TiO_2. When titanium dioxide is irradiated with light that exceeds its bandgap energy (3.2 eV for anatase) i.e. UV light (wavelength <385 nm for anatase), electron-hole pairs are created. The electron-hole pairs degrade organic pollutants on the catalyst surface either directly or indirectly in a water solution by creating hydroxyl and superoxide radicals (Hoffmann *et al.*, 1995). An energy diagram of the creation of electron hole pairs is shown in Fig. 2.2. This diagram demonstrates the various steps in the photocatalysis process. The first step is the formation of charge carriers (electron hole pairs) by a photon (1). The most likely next step is electron hole pair recombination to liberate heat given that the quantum yield for the reaction is only about 0.04–0.05. This means that the electron hole pair recombine 96 % of the time (Zhou and Smith, 2002) (2); If recombination does not occur, an oxidative pathway by a valence-band hole will occur (3); A reduction pathway by a conduction-band electron to complement step (3) at (4); Further ROS

and photocatalytic reactions yield intermediates and potentially mineralisation products (5). It is also possible for the trapping of a conduction-band electron in a surficial molecule to yield Ti (III) (6) and trapping of a valence-band hole at a surficial titanol group (7).

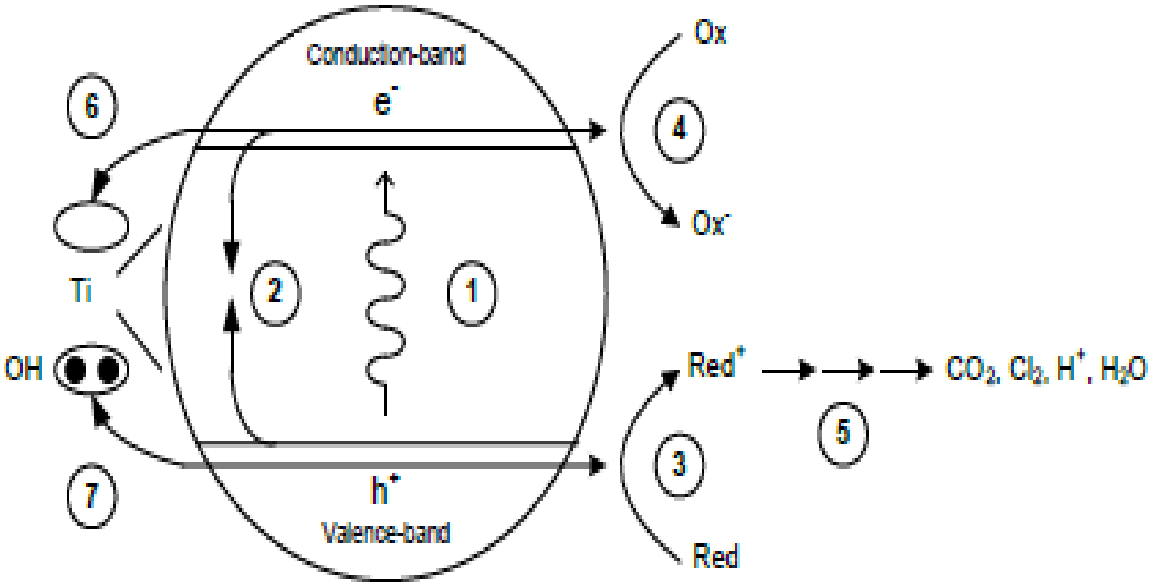


Fig. 2.2.Proposed mechanism of Photocatalysis. Hoffmann *et al.*, (1995); Peralta-Hernández et al., (2007)

The chemical reactions occurring at the catalyst surface (steps 3 and 4 in Fig. 2.2) have been summarised (Benabbou *et al.*, 2007; Kim *et al.*, 2005). An electron is excited from the valence band (VB) to the conduction band (CB). This process results in a positive region in the VB hole (h+) and a free electron (e-) in the CB. (Eq. 2.1):

$$T_iO_2 \xrightarrow{hv} T_iO_2 + e^-(CB) + h^+(VB) \qquad (2.1)$$

The hole at the catalyst surface reacts with hydroxyl ions (OH-) and adsorbs water to form hydroxyl free radicals (•OH) (Eqs. 2.2 and 2.3):

$$T_iO_2(h^+) + OH^- \rightarrow T_iO_2 + {}^{\cdot}OH \qquad (2.2)$$

$$T_iO_2(h^+) + H_2O_{ads} \rightarrow T_iO_2 + {}^{\cdot}OH + H^+ \qquad (2.3)$$

The CB electron reduces oxygen to the superoxide ion: O_2•- (Eq 2.3). This reaction prevents the e-/h+ recombination, in the absence of other electron acceptors (pollutants).

$$O_2 + e^- \rightarrow O_2^{\cdot-} \quad (2.4)$$

The further reduction of O2•- produces H_2O_2, as described in Eq. (2.5)

$$O_2^{\cdot-} e^- 2H^+ \rightarrow H_2O_2 \quad (2.5)$$

The superoxide ion and its protonated form subsequently dismute to yield hydrogen peroxide or a peroxide anion (Eq's. 2.6 – 2.8):

$$O_2^{\cdot-} + H^+ \rightarrow HO_2^{\cdot} \quad (2.6)$$

$$O_2^{\cdot-} + 4HO_2^{\cdot} \rightarrow 2\ {}^{\cdot}OH + 3O_2 + H_2O_2 \quad (2.7)$$

$$2HO_2^{\cdot} \rightarrow O_2 + H_2O_2 \quad (2.8)$$

The addition of H_2O_2 can increase the photodegradation rate under certain conditions, probably by the formation of •OH radicals via the Harber–Weiss reaction (Eq. 2.9) or through the reduction of H_2O_2 by the CB e- (Eq. 2.10)

$$O_2^{\cdot-} + H_2O_2 \rightarrow\ {}^{\cdot}OH + OH^- + O_2 \quad (2.9)$$

$$H_2O_2 + e^- \rightarrow\ {}^{\cdot}OH + OH^- \quad (2.10)$$

Recombination of •OH radicals can also lead to the production of hydrogen peroxide (Eq. 2.11):

$${}^{\cdot}OH +\ {}^{\cdot}OH \rightarrow H_2O_2 \quad (2.11)$$

It is suggested that H_2O_2 production ceases in the absence of O_2. Of all the ROS generated the •OH radical is the most important oxidant species since it has the very high positive redox potential as shown in Table 2.8.

Table 2.8. Redox potential for oxidizing agents in water

Oxidative species	Redox potential (V) vs. NHE	Redox potential relative to chlorine
Fluorine (F^-)	3.06	2.25
Hydroxyl radical (•OH)	2.80	2.05
Oxygen (atomic)	2.42	1.78
Ozone (O_3)	2.08	1.52
Hydrogen peroxide (H_2O_2)	1.78	1.30
Permanganate (MnO_4^-)	1.69	1.24
Hypochlorite (ClO^-)	1.49	1.1
Chlorine (Cl^-)	1.36	1.00
Oxygen (molecular)	1.23	0.9

Source: Al-Kdasi *et al.*, (2004); Zhou and Smith, (2002)

2.4 Zinc ferrite and its composites as photocatalysts.

Spinel zinc ferrite $Znfe_2O_4$ is a semiconducting material with tetrahedral sites occupied by Zn^{2+} ions and octahedral sites by Fe^{3+} (Klimkeiwicz*et al*., 2009). The conduction mechanism in zinc ferrite is due to the Fe^{2+} and Fe^{3+} ions present in octahedral sites as suggested by Feteira *et al*.,

(2009). Its chemical and thermal stability has made zinc ferrite important materials, such as magnetic materials, catalysts and absorbent materials and its band gap is small (1.9 eV) due to which it utilizes visible light to act as a photocatalyst (Yogoand Ishikawa, 2000).

The advantage of ferrites as photo catalysts is their capability to absorb visible light solar irradiation because of low band gap and large availability of catalytic sites for adsorption of noxious waste and dyes (Tsukada*et al*., 2008). Also, ferrites are magnetic in nature giving them added advantage of easy recovery after photocatalytic reaction. Zinc ferrite semiconductor photocatalyst has been applied widely to degrade the organic pollutants for the remediation of hazardous wastes, contaminated groundwater, the control of toxic air contaminants, self-cleaninig, self-sterilizing surfaces, photocatalytic metal corrosion prevention and photocatalytic lithography (Hoffmann *et al*., 1995). Zinc ferrite has potential applications in the conversion of sunlight and sensitive towards visible light (Ehrhardt *et al*., 2003).

Zinc ferrites have also been used in combination with other photocatalysts, including TiO_2, in an effort to enhance photocatalytic activity. When combined with TiO_2, the composite photocatalysts that are formed show higher efficiency as photocatalysts than the individual Zinc ferrite or TiO_2 alone. The composites are commonly prepared as a mixed powder, where TiO_2 is coupled with ferrite nanoparticles (Zhang *et al*., 2008), as a film in which a TiO_2 film is doped with ferrites (Qui *et al*., 2004) or as a single nanoparticle with the ferrite acting as a magnetic core and the TiO_2 as a shell (Kostedt *et al.*, 2005). The combination of ferrites with TiO_2 shows a synergistic effect that produces enhanced photocatalytic activity leading to more effective degradation of contaminants. Also, with the addition of ferrites to TiO_2, the composites become effective under visible light irradiation, whereas TiO_2 alone is effective only under UV light. Other compounds have also been combined with ferrites in order to gain similar effects and

enhance photocatalytic activity. These include ZnO (Kaneva and Dushkin,2011) Ag, (Zhu *et al.,* 2010) Ag_3VO_4, (Cheng *et al*., 2004), multi-walled carbon nanotubes (Chen *et al.,* 2010), WO_3 (Liu *et al.,* 2009), $Bi1_2TiO_{20}$ (Xu *et al.,* 2007), and $PbBi_2Nb_2O_9$ (Kim *et al.,* 2005)among others. Each study focused on enhancing the photocatalytic activity by preparing a composite capable of absorbing visible light. In each case, the degradation of contaminants in water was studied with promising results.

The purpose of combining photocatalysts is to decrease the recombination of e-/h^+ pairs and also to convert them to be active in the visible region spectrum which is shown in Fig. 2.3. Combining two photocatalysts, each with different band gap positions, can effectively cause a greater separation of the e^-/h^+ pairs, thereby allowing more of these species to be available for the oxidation and reduction reactions that lead to mineralization of pollutants.

2.5 Synthesis of ferrites

A number of different methods including thermal methods, sol– gel and citrate methods, co-precipitation, solid-state reactions, and many others are used to prepare ferrites. Fig. 2.3describes the different methods used to prepare ferrites with a spinel structure, all of which use Fe(III) and M(II) salts as precursors.

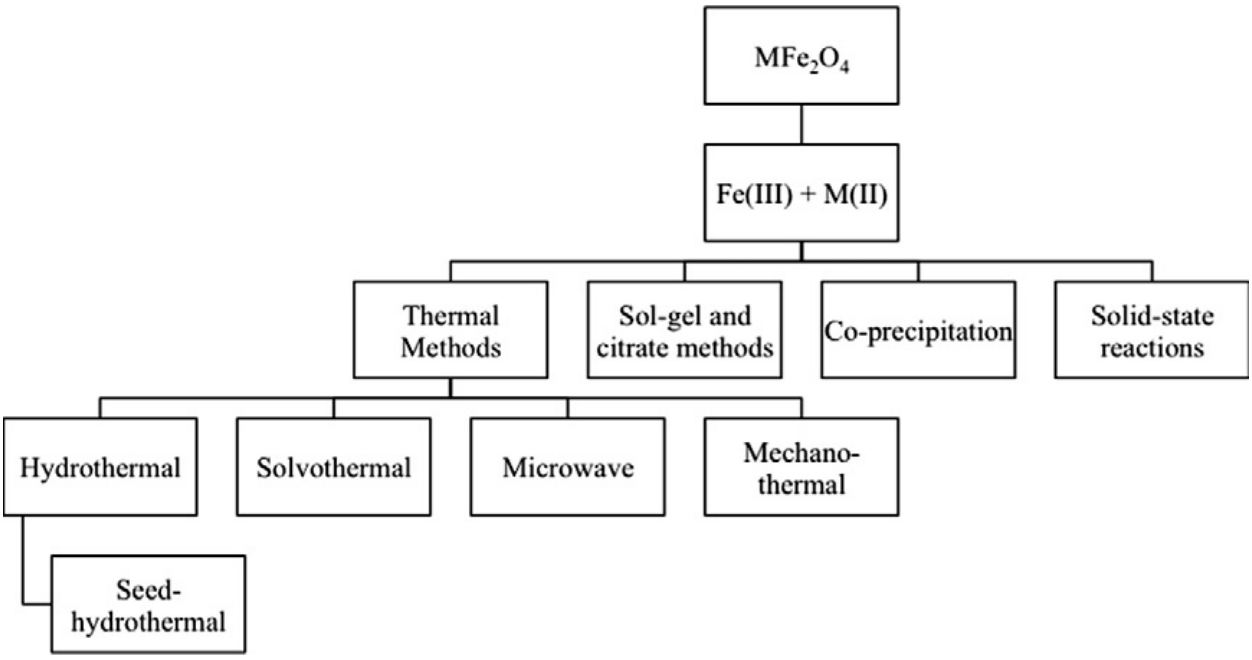


Fig. 2.3. Preparation methods of ferrites using Fe(III) and M(II) salts as precursors. Zhang *et al*., (2011)

2.5.1 Thermal methods. The thermal synthesis of ferrites are hydrothermal (Sue *et al.,* 2011) solvothermal (Liu *et al.,* 2011), microwave (Dom *et al.,* 2011) mechano thermal (Fu*et al.,* 2010), and seed-hydrothermal (Farbod and Khademalrasool, 2011). In each of these methods an iron salt is used, usually Fe (- $NO_3)_3$-$9H_2O$ or $FeCl_3$-$6H_2O$, and a salt of the metal that is used, commonly M-$(NO_3)_2$, M-SO_4, or M-Cl_2. Salts are dissolved in water or another solvent under stirring and the pH is adjusted to between 7 and 12, depending on the metal salt that is used. The mixture is placed into an autoclave and heated for 12–24 h, followed by naturally cooling to room temperature. The solid is collected by filtration or centrifugation and washed, followed by drying at approximately 85 ^{0}C overnight. For mechano-thermal treatment, rather than dissolving, the precursor compounds are ground together in a ball-mill using the same basic procedure. Seed-hydrothermal techniques use a seed of the metal oxide (M_2O_3) with the Fe(III) salt. The two compounds are placed into an autoclave and heated, and using the same procedure as described above.

2.5.2 Sol–gel and citrate methods

Sol–gel and citrate methods involve the addition of the metal and iron precursors, along with citric acid, to form a gel. The precursors are dissolved in water or ethanol and stirred vigorously at pH 9 until a gel-like material is formed. Citric acid assists in the homogeneous distribution of the metal ions into solution. The gel is dried and then sintered at temperatures ranging from 450–800 ^{0}C at various periods of time. The sintering time is normally varied and tested to determine the effects on the photocatalytic activity (Pardeshi and Pawar, 2011; Kaneva and Dushkin, 2011).

2.5.3 Co-precipitation methods

Co-precipitation methods to prepare ferrites are similar to thermal methods. Fe (III) and metal salts are dissolved in water along with a surfactant, oleic acid, under stirring and gentle heating. The reaction mixture pH is increased to 7–10 in order to precipitate the ferrite particles. The solid nanoparticles are filtered and washed with DI water and/or ethanol and subsequent drying at 80 – 100 ^{0}C. Once dried, the nanoparticles can then be calcined at various temperatures to determine the effects of the high temperature on the activity of the nanoparticles (Zhang *et al.,* 2011; Jadhav*et al.,* 2010)

2.5.4 Solid-state reactions

Solid-state reactions involve heat-treating powders of the iron and metal salts. For example, to synthesize $CaFe_2O_4$, Fe_2O_3 and $CaCO_3$ powders are mixed and then heated to 1100 ^{0}C for 2 h. (Cheng *et al.,* 2004).

$$CaO + Fe_2O_3 \rightarrow CaFe_2O_4 \quad (2.12)$$

$$2FeO + H_2O \rightarrow Fe_2O_3 + H_2 \quad (2.13)$$

$$CaO + CO_2 \rightarrow CaCO_3 \quad (2.14)$$

2.6 Visible Light Photocatalysis

The solar irradiance has significant intensities in the visible light region as shown in Fig. 2.4. For this reason, efficient photocatalysis applications relying on solar irradiance require visible light-responsive photocatalysts.This requirement is even more significant for indoor photocatalysis applications. Ferrites are visible light responsive Photocatalyst due to their low band gap. The band gaps (3–3.2 eV) of convensional photocatalysts such as TiO_2 and ZnO, which absorb from the UV region of the solar spectrum, are their major drawbacks in photocatalysis because only about 5% of sunlight comprises UV radiation as shown in Fig.2.3. Modification of the band gap in nanocrystalline titanium dioxide is, therefore, a well-studied research area. Modifications can be effected either in bulk or on the surface of TiO_2. Surface modifications are usually achieved by anchoring colored inorganic semiconductors (Wang *et al.*, 2009) or organic dyes on the TiO_2 surface (Bach *et al.*, 1998), where they act as sensitizers. However, most of these sensitizers are susceptible to photocorrosion or degradation in aqueous solutions and are not suitable for photocatalytic water-treatment applications. Instead, they are good candidates for solar cell devices.

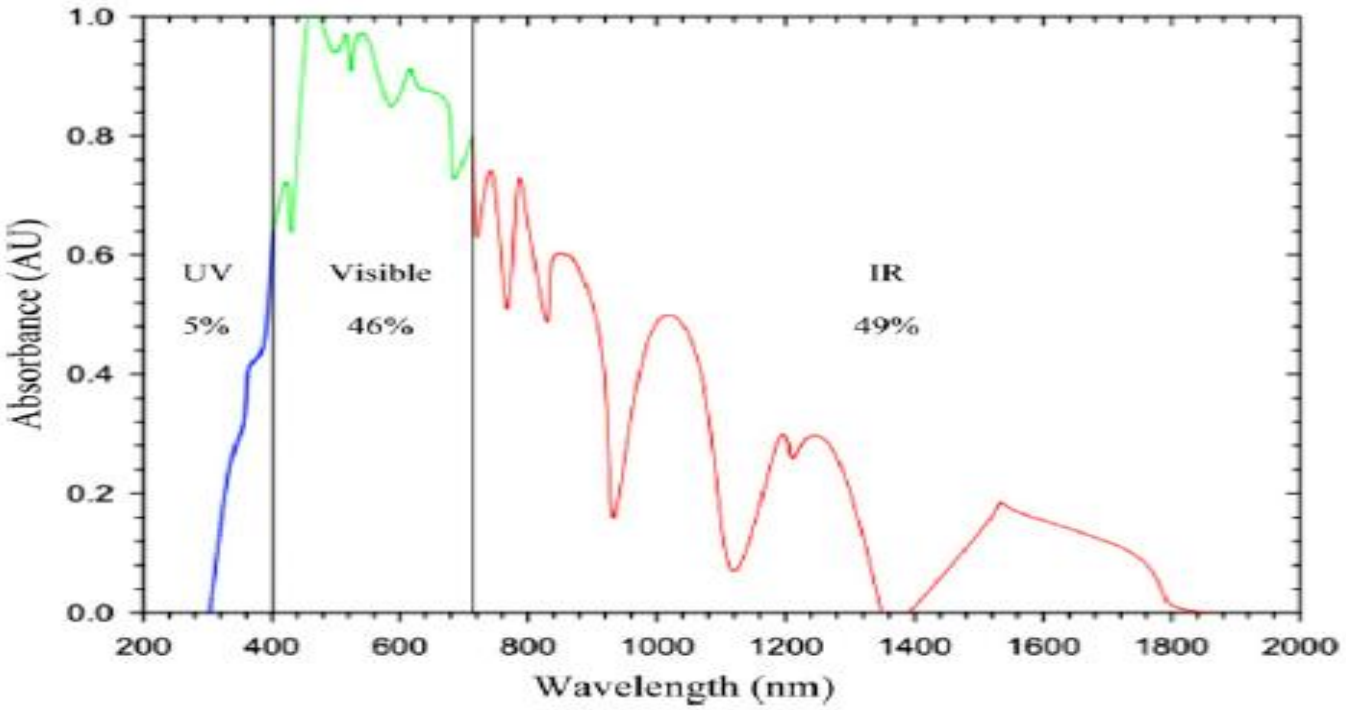


Fig. 2.4. The solar spectrum (ASTM: **www.astm.org**)

2.7 Applications of photocatalytic processes

Photocatalytic processes are widely recognized as viable solutions to environmental problems (Yogo and Ishikawa, 2000; Ljubas, 2005). The semiconductors commonly used in photocatalytic processes are nontoxic, chemically stable, available at a reasonable cost, and capable of repeated use without substantial loss of catalytic ability (Fujishima*et al.,* 2000). Heterogeneous photocatalysis is a safe, nonhazardous, and ecofriendly process which rarely produce any harmful byproducts. Extensive research in this field has been done in the area of photocatalytic removal of organic, inorganic, and microbial pollutants (Fujishima *et al.,* 2000; Rincon and Pulgarin, 2005). Some of the applications of photocatalysis are presented in Table 2.9.

Table 2.9. Applications of Photocatalysis

Application	Examples
Water Purification	Decontamination of river water, ground water, lakes, industrial wastewaters, airport and agricultural wastewater, pool water, fish feeding tanks, water disinfection, oil spill remediation, killing micro-organisms and pathogens in water, etc.
Air Purification	Room air cleaners, air conditioning, tunnel and buildings air purification, deodorization and disinfection of indoor air, air cleaning units for refrigerators, etc.
Self-cleaning surfaces	Window blinds, exterior tiles, kitchen and bathroom components, plastic surfaces, traffic signs and reflectors, tent materials, building windows, spray coating for cars, indoor lamp covers, etc.
Self-sterilizing surfaces	Titles and coatings to cover floor and walls in operating rooms, hospital uniforms, public restrooms, pet-breeding rooms.
Photocatalytic metal corrosion prevention	Metal corrosion prevention using TiO_2 photo anodes, photocatalytic coating of TiO_2 on metal surface for corrosion prevention, etc.
Photocatalytic Lithography	Development of alternative lithographic process utilizing photocatalysis.
Water splitting	Water splitting for the production of hydrogen from water using photocatalysis.
Petrochemical production	Conversion of carbon dioxide into gaseous hydrocarbons and methanol in the presence of water. Desulfurization of petroleum fraction. Decomposition of Polyaromatic hydrocarbons (PAHs)

Source: Amadelli *et al*., (2008)

2.8 Kinetics of photocatalytic processes

The kinetics of heterogeneous photocatalytic degradation of aqueous pollutants by composite photocatalyst is still a subject of debate (Wang et al., 2009; Tian*et al.,* 2009). Several recent reports claim that it follows the Langmuir-Hinshelwood (L-H) kineticsmodel (Lin *et al.,* 2009). The linearized form of L-H model is given by eq. 2.15 (Hamza *et al.,* 2013).

$$\frac{1}{r_0} = \frac{1}{k_r \mathrm{K}_L C_0} + \frac{1}{k_r} \qquad (2.15)$$

where r_0 is the initial reaction rate, C_0 is the initial concentration of the substrate, k_r is the intrinsic photocatalytic reaction rate constant ($mgl^{-1}min^{-1}$) .

$$r = -\frac{dC}{dt} = k_{LH} K_L C_{eq} = k_{app} C_{eq} \qquad (2.16)$$

At low concentrations of pollutant, $K_L Ceq$ ($K_L C_{eq} << 1$) is negligible and equation (2.16) becomes a pseudo-first-order rate expression (Lin *et al.,* 2009).

Integrating Equation (2.16)

$$\frac{C}{C_{eq}} + constant = k_{app} t \qquad (2.17)$$

Equations (2.16) and (2.17) account for the adsorption of the reactant (pollutant) only but do not consider the adsorption on nano tube oxidation of any intermediates or products formed during the course of the degradation reaction.When the adsorption of intermediates or products must be considered (Sirtori, *et al.,* 2009), a modified rate equation results is given by:

$$r = -\frac{dC}{dt} = k_{LH} \frac{K_L C_{eq}}{1 + K_L C_{eq} + \sum_{i=1}^{n} K_i C_i (i = 1, n)} \qquad (2.18)$$

Where, $k_i$and $C_i$are the adsorption constant and concentration of intermediates at any given time, respectively. When the initial concentration of pollutants is very low, $1 + K_L C_{eq} + \sum_{i=1}^{n} K_i C_i (i =$

$1, n$) is negligible and the reaction follows pseudo-first-order kinetics, as shown in Equations (2.16) and (2.17).

Sirtori *et al.*(2009)have reported that the photocatalytic degradation by nanocrystalline titanium dioxide follows L-H kinetics at low pollutant concentrations and below the catalyst saturation level. It deviates from the pseudo-first-order kinetics under several conditions. The photocatalyst concentration and the light flux have been found to influence the degradation kinetics of some pollutants (Lin *et al.*, 2009). According to the L-H model, the photocatalytic degradation rate of organic pollutant should increase with an increase in the photocatalyst loading because of the additional available active sites (θ) for adsorption. This was observed up to a certain catalyst loading (catalyst saturation), but above that limit, the experimental kinetics results did not fit the L-H model (Lin *et al.*, 2009). This was mainly ascribed to three reasons, at higher photocatalyst loading, (i) deactivation of activated photocatalyst could occur upon collision with ground state photocatalysts, (ii) there is a higher possibility of agglomeration and sedimentation of photocatalyst, and (iii) there is decreased light penetration through the reaction medium.

Light flux has been found to be an important influence on the degradation kinetics of methylparaben in aqueous medium (Lin *et al.*, 2009). At low UV light flux (1.2×10^{15} photons s^{-1} $cm^{-2} < \Phi < 4.0 \times 10^{15}$ photons s^{-1} cm^{-2}), methylparaben degradation followed L-H kinetics, where electron-hole pairs mainly resulted in chemical reactions rather than recombination. However, at intermediate UV light intensities (4.0×10^{15} photons s^{-1} $cm^{-2} < \Phi < 5.8 \times 10^{15}$ photons s^{-1} cm^{-2}), the methylparaben degradation rate is varied as a functional order between zero and one. In this medium UV light region, the recombination of electron-hole pairs was predominant over degradation.

The random selection of a particular concentration of the pollutant is not enough to study the dependence of rate on photon flow (Emeline *et al.,* 2005). Concentration of the pollutant is also important as demonstrated by Serpone *et al.* (Emeline *et al.,* 2005). Where, the order of the photocatalytic reaction varied between zero (at low pollutant concentration) and one (at high pollutant concentration) in the same range of light irradiance. Therefore a complete study should focus on different concentrations of pollutant to know the dependence of light irradiance on the photocatalytic reaction rate.

Wang *et al.,* (2012) developed a rate expression that was different from the conventional pseudo-first-order rate equation, to explain the kinetics of sulfosalicylic acid degradation in aqueous solution using nanocrystalline Photocatalyst. Their proposed rate equation considers factors such as the lifetime and concentration of ·OH, pH, and adsorption of intermediates on photocatalyst. The rate equation can be represented as follows.

$$-\frac{dC}{dt} = \frac{k_{+3}k_4\tau h^+}{k_{-3}[H^+]}\frac{K_L C_{eq}}{1+\sum_{i=5}^{n} K_i C_i + K_a C_{eq}} \tag{2.19}$$

$$\frac{k_{+3}[h^+]}{k_{-3}[H^+]} = [\ \cdot OH] \tag{2.20}$$

Where, τ is the lifetime of ·OH and k_4 is the rate constant for the reaction of ·OH with the adsorbed pollutant on photocatalyst. *KQ* and *Ki* are the adsorption equilibrium constants of sulfosalicylic acid and the intermediates, respectively, and *Ceq* and *Ci* are their equilibrium concentrations. Adsorption of the identified intermediates of sulfosalicylic acid degradation on nanocystalline titanium dioxide was found to be insignificant (Wang *et al.,* 2012). Hence, Equation (2.21) can be simplified as

$$-\frac{dC}{dt} = \frac{k_{+3}k_4\tau h^+}{k_{-3}[H^+]}\frac{k_a C_{eq}}{1+K_a C_{eq}} \tag{2.21}$$

Integrating Equation (2.23), yields

$$\ln\left(\frac{C_{eq}}{C}\right) + K_a\left(C_{eq} - C\right) = k_{app}t \qquad (2.22)$$

The order of the degradation reaction will then be determined by three different adsorption situations: (i) weak adsorption ($KQ\ C_{eq} << 1$); (ii) medium adsorption ($0.1 < KQ\ C_{eq} < 10$), and (iii) strong adsorption ($KQ\ C_{eq} > 10$) (Wang et al., 2009). In the case of weak adsorption of the pollutant on nanocrystalline titanium dioxide, Equation (2.16) reduces to the pseudo-first-order expression, as shown in Equation (2.23). Medium adsorption leads to Equation (2.22), which was observed in the case of sulfosalicylic acid degradation kinetics. In the case of strong adsorption, the rate is independent of *KQ* and adsorption does not affect the rate of the reaction; here, the reaction will follow a zero-order kinetic model and the rate expression becomes

$$\ln\frac{C_{eq}}{C} = k_{app} \qquad (2.23)$$

Where, K_{app} is the pseudo - first order rate constant (min^{-1}), C_{eq} is initial concentration, Cis the concentration at time t (min).

The rate of photocatalytic degradation of some pollutants may also depend on other factors such as alkalinity, and the presence of natural organic matter (Pelaez *et al.,* 2011). Especially in the real systems, Carbonate and bicarbonate ions, which are responsible for the alkalinity of water, have been found to decrease the rate of the photocatalytic degradation of microcystine-LR. Also, the presence of humic acid and fulvic acid (natural organic matter) reduced the rate of microcystine-LR degradation (Pelaez *et al.*, 2011).

2.9 Characterization of solid photocatalysts

2.9.1 Surface area analysis using sear's method.

The surface area of synthesized nanoparticles is commonly determined using a Brunaur–Emmett–Teller (BET) surface analyzer. The smaller particles have a larger surface area, leading to higher photocatalytic activity due to a larger number of active sites.

2.9.2 Crystal phase structure analysis.

X-ray diffraction (XRD) is often used to determine the crystal phase structure of crystalline solids. The XRD measures the diffraction pattern of the crystal structure (2H) at different intensities, which give insight into the type of crystal lattice formed. Each ferrite has a different diffraction pattern due to the different metal cation present in the structure. These cations are different sizes, and therefore as the X-ray passes through the material diffract differently, thus giving each a unique spectrum. The obtained deffractogram, as shown in Fig. 2.8, is compared with a known standardusing the Joint Committee on Powder Diffraction Standards (JCPDS) index cards.

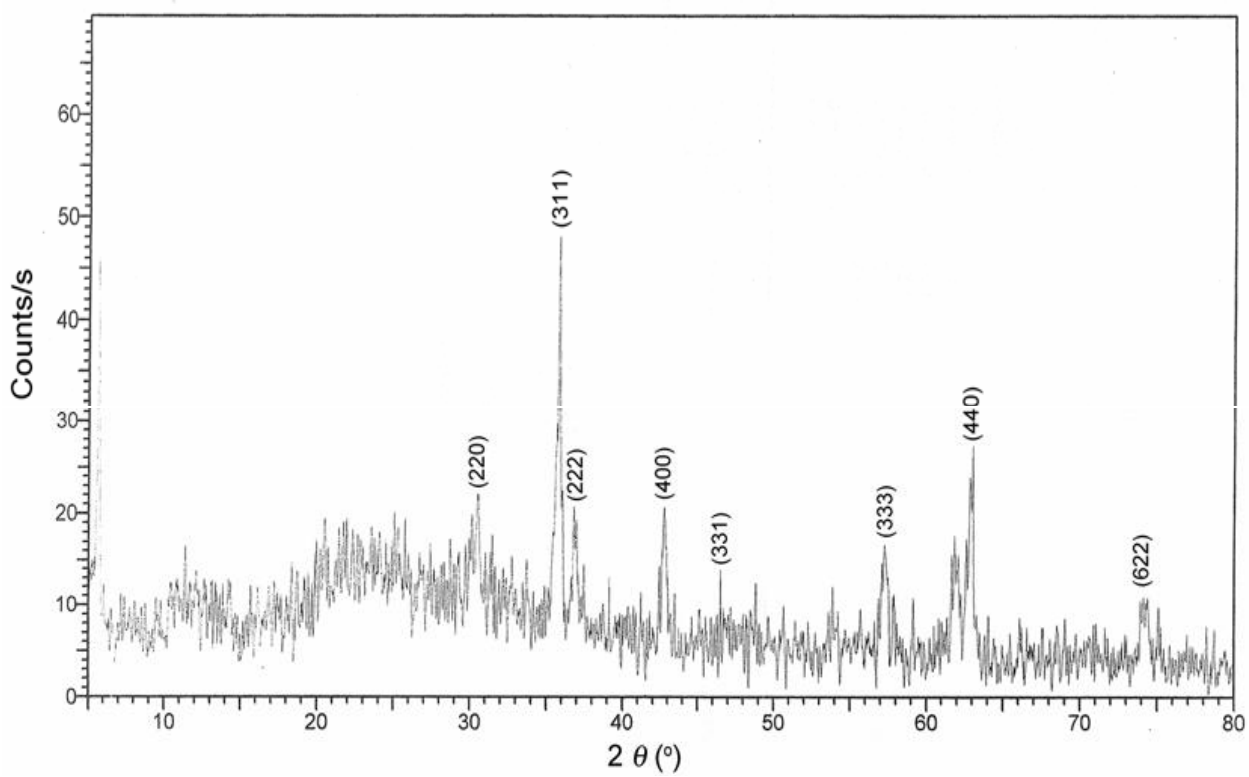


Fig. 2.5.Typical XRD pattern of $ZnFe_2O_4$ Prithviraj Swamy *et al.*, (2010).

2.9.3 Surface morphology analysis.

Scanning-electron microscopy (SEM) and transmission electron microscopy (TEM) are frequently used to determine the surface morphology of solids. Typical SEM and TEM images for $ZnFe_2O_4$prepared via co-precipitation route are shown in Fig. 2.6a and b. The size and shape of the photocatalytic particles are determined from the obtained images. This information gives insight into how different preparatory methods affect the structures. For example, it is possible to determine if the prepared photocatalyst is a powder with no defined structure (Dom *etal.*, 2011), with a defined structure such as nanospheres (Li *et al.*, 2011)or a film on a substrate (Qui et al., 2004). Similarly, preparing the photocatalyst by the citrate–nitrate method or by thermal methods gives a different shape to the nanoparticles, which can be seen using these techniques (Yang *et*

al., 2007). SEM and TEM images can also be studied after the use of photocatalyst to determine if any decomposition occurs.

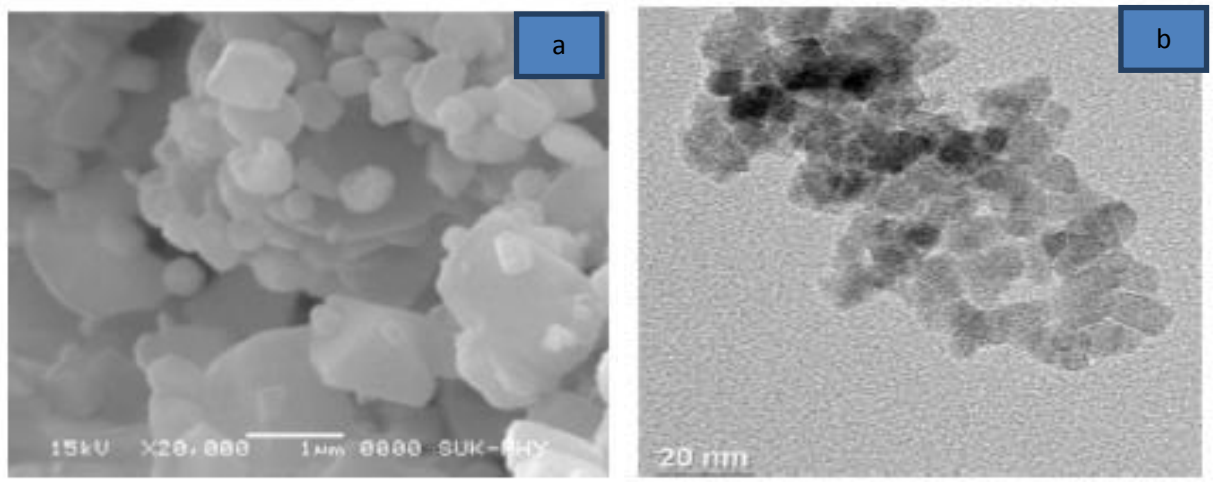


Fig. 2.6. (a) SEM image of $ZnFe_2O_4$ reported by Jadhav *et al.*, (2010) and (b) TEM image of $ZnFe_2O_4$ reported by Chen *et al.*, (2010)

2.10 Methylene blue (MB)

Methylene Blue (methylthionine chloride) is a heterocyclic aromatic chemical compound with molecular formula shown in Fig. 2.7. MB is a cationic thiazine dye that is deep blue in the oxidized state while it is colorless in its reduced form (leucomethylene blue). It is one of the common dyes that have been studied as a model compound for organic contaminants. MB dye is commonly used in chemistry as a redox indicator as well as in biology as a stain and in textile industries as a coloring agent. The structure of MB shown in Fig. 2.7, contain a phenothiazin with a dimethyl amine on each side. MB dye tends to show relatively high degradation potential with ferrites both alone as well as when combined with other photocatalysts (Wiklund *et al.*, 2007).

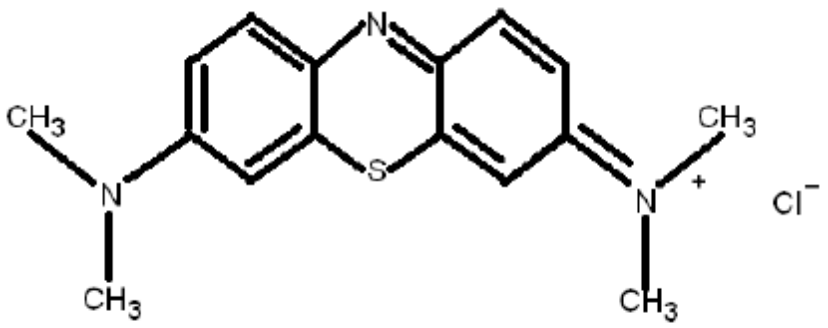


Fig. 2.7. Structure of MB, Disanto and Wagner, (1972)

Table 2.10summarizes the results of studies of the degradation of MB dye with ferrite photocatalysts. MB dye is highly degraded by ferrites when in combination with other photocatalysts. The degradation efficiency of the dye varies depending on the ratios of the photocatalysts as well as with temperature treatments, both before use, as well as in the preparation process. Another aspect that has been studied is the effect of ball-milling on photocatalysts. It can be seen that a composite photocatalyst of ZnO with 1% $CaFe_2O_4$ degrade 73% of the dye solution with no external treatment. When a photocatalyst is ball milled at different times, the degradation efficiency changes. At 3 h, the degradation drops to 50.8%, after 6 h, there is an increase to 73.4% and then a maximum of 78.7% is reached at 12 h (Cheng *et al.*,2004).This shows that mechanical treatment of the photocatalyst can have a significant effect on the photocatalytic activity. Another study on the degradation of MB dye involved the addition H_2O_2 to the reaction mixture. As discussed in Eqs. (2.3) – (2.11), the H_2O_2 creates a Fenton-type system, which causes a larger number of reactive oxygen species formations, and therefore results in much high reactivity. This fact is evident as seen with $ZnFe_2O_4$ and H_2O_2 without light irradiation, which shows a 45% degradation of the dye. When irradiated with light, degradationis increased to 52%, showing that H_2O_2 can play an important role in the

photocatalytic process (Chen*et al.,* 2009). Composite photocatalysts also show increased degradation efficiency with the addition of H_2O_2. A $ZnFe_2O_4$ and multiwalled carbon nanotube (MWCNTs) composite photocatalyst alone shows 25% MB dye degradation, however when H_2O_2 is introduced, there is an increase to 99%. Another important study that deserves mention is, as can be seen in Table 2.8 the addition of a metal to Fe_3O_4, which when used alone in the presence of H_2O_2 has only 10% MB dye degradation efficiency. However, adding metals such as Ni ($Fe_{2.46}Ni_{0.54}O_4$) or Mn ($Fe_{2.47}Mn_{0.53}O_4$) increase the MB degradation to 99% efficiency (Liu *etal.,* 2009).

Table 2.10. Ferrites and mixed ferrites reacted with MB (Fu *et al*., 2010)

Photocatalyst	**Dye (mg/L)**	**Catalyst (g/L)**	**Irradiation time (min)**	**irradiation source**	**Degradation (%)**
$Ag_3VO_4/CaFe_2O_4$ (1.0%)	32	2.0	60	k > 470 nm	66.4
$Ag_3VO_4/CaFe_2O_4$ (2.0%)	32	2.0	60	k > 470 nm	79.1
$ZnO/CaFe_2O_4$ (0.1%)	32	2.0	20	UV	57
$ZnO/CaFe_2O_4$ (0.5%)	32	2.0	20	UV	68
$TiO_2/CoFe_2O_4$ (10%)	5	0.1	60	UV	56
$TiO_2/CoFe_2O_4$ (20%)	5	0.1	60	UV	60
TiO_2/Ni-Cu-Zn ferrite	20	1.33	120	UV	82
$ZnFe_2O_4$	10	0.6	180	400–700 nm	32
$MnFe_2O_4$	7	0.3	1200	Visible	67.18
$ZnFe_2O_4$/MWCNT	10	1 3	60	k > 420 nm	25
Photocatalyst	Dye (mg/L)	Catalyst (g/L)	Irradiation time (min)	irradiation source	Degradation (%)
$Ag_3VO_4/CaFe_2O_4$ (1.0%)	32	2.0	60	k > 470 nm	66.4
$Ag_3VO_4/CaFe_2O_4$ (2.0%)	32	2.0	60	k > 470 nm	79.1
$ZnO/CaFe_2O_4$ (0.1%)	32	2.0	20	UV	57
$TiO_2/CoFe_2O_4$ (10%)	5	0.1	60	UV	56
$TiO_2/CoFe_2O_4$ (20%)	5	0.1	60	UV	60
TiO_2/Ni-Cu-Zn ferrite	20	1.33	120	UV	82
$ZnFe_2O_4$	10	0.6	180	400–700 nm	32
$MnFe_2O_4$	7	0.3	1200	Visible	67.18
$ZnFe_2O_4$/MWCNT	10	1 3	60	k > 420 nm	25

2.11 α-Alumina

Alumina is the raw material used in the production of many different types of ceramic materials, catalyst supports and refractories. Generally, there are two types of alumina, the lower grade alumina and the technical grade alumina. Lower grade alumina is of low purity and is produced as a starting material for making aluminium metal. Technical grade alumina is a high purity ceramic alumina and is used in high technology applications. Basically, there are two types of commercial technical alumina, which are gamma and alpha alumina. There is a high demand for high-tech ceramic materials with properties better than most metals. Alumina is one of the high-tech ceramic materials that are widely used (Nagaveni *et al*., 2005).

Alumina in the alpha crystal form ranks next to silicon carbide and diamond in terms of hardness and is used as cutting tools, polishing and bullet-proof, catalyst and support materials. Alpha alumina on the other hand is stable even at very high temperature and is used as thermal barriers, catalyst support, insulator abrasives; in electronics, structural, coating as synthetic sapphires and as translucent bodies. Commercial technical grade alpha alumina contains a minimum 90% of alpha alumina and a maximum 10% of gamma alumina (Manova*et al*., 2011).

2.12 Some Previous Related Works

Sesha *et al*., (2006) synthesized and characterized the TiO_2 – $ZnFe_2O_4$ nanocomposite. It was observed that the narrow band gap semiconductor $ZnFe_2O_4$ can be effectively coupled with TiO_2 for visible – light (> 400nm) activated photocatalysis because it showed the potential of inexpensive and nontoxic photocatalysts for indoor visible – light applications. Jadhav *et al.*, (2010) studied the effect of sintering on photocatalytic degradation of methyl orange using $ZnFe_2O_4$ as photocatalyst. They observed that the $ZnFe_2O_4$ nanoparticles sintered at 500 ^oC and

irradiated for 60min shows highest activity than those calcined at the following temperature of 600 ^{o}C, 700 ^{o}C, 800 ^{o}C, and 900 ^{o}C.

Rong *et al.,* (2012) prepared and characterized the magnetic $ZnFe_2O_4$ Core – Shell@ZnO Nanoparticles and applied them for the photodegradation of MB. It was concluded that the prepared $ZnFe_2O_4$@ZnO sample at a ratio of (1:10) exhibited higher Photocatalytic efficiency than pure $ZnFe_2O_4$.Sonal *et al.,* (2013) enhanced Photocatalytic degradation of MB using $ZnFe_2O_4$/MWCNT composite synthesized by hydrothermal method. This clearly indicated the enhancement of Photocatalytic activity in $ZnFe_2O_4$/MWCNT nanohybride. It was observed that MB was almost 84% degraded in the presence of $ZnFe_2O_4$ while 99% degradation was observed in case of $ZnFe_2O_4$/MWCNT nanocomposite after irradiation for 5 hrs. Ping *et al.,* (2014) studied the Physical and photocatalytic properties of $ZnFe_2O_4/TiO_2$ under visible light irradiation and observed that the $TiO_2/ZnFe_2O_4$ has effectively photodegraded methyl orange under visible light irradiation and concluded that sample has best surface area and surface charge when calcined at 400 ^{o}C.

Dutta *et al.,* (2014) studied the efficient solar photocatalytic degradation of textile wastewater using ZnO/ZTO composite and the solar degradation efficiency of wastewater (50% degradation) that can be due to the mixture of dyes in textile wastewater. Jumeri *et al.,* (2014) studied the microwave synthesis of magnetically separable $ZnFe_2O_4$ – reduced graphene oxide for wastewater treatment and observed that after 2 hrs of absorbtion at 664 nm, the amount of MB removed by Fe_3O_4 was 7%, 15% by $ZnFe_2O_4$ 19% by ZnO, 29% by ZnO-rGO, 60% by Fe_3O_4-rGO and 82% by the $ZnFe_2O_4$ – rGO nano – composite.

CHAPTER THREE

MATERIALS AND METHODS

3.1 The following is the list of materials and equipment used in this work. All chemicals listed were obtained from Stevemore chemical store in Zaria, Nigeria.

3.2 Materials and equipment

1. Zinc Chloride. (Analytical grade, BDH Chemical England)
2. Iron (III) Chloride. (Analytical grade, BDH Chemical England)
3. Sodium Hydroxide. (Analytical grade, BDH Chemical England)
4. α - alumina. (Analytical grade, BDH Chemical England)
5. Textile effluent obtained from African Textile industry Kano
6. Methylene Blue(KLT Laboratory Mumbai India)
7. Conical Flask (500 ml, 2000 ml) Pyrex.
8. Beaker (5000 ml) Pyrex.
9. Measuring Cylinder (1000 ml, 500ml).
10. Spatula.
11. Filter Paper.
12. Sinta Glass Filter (Quick fit TM).
13. Funnel.
14. Water Bath.
15. Glass Rod Stirrer.
16. Crucibles.
17. Thermometer.
18. Retort stand.

Other equipment used are presented in Table 3.1

Table 3.1. List of equipment used and their specifications

S/No	Name	Model	Manufacturer
1.	Hot Plate and Magnetic Stirrer	C1202	Thermocool, England
2.	Digital Weiging Balance	AB 204 (0 – 180g)	Mettler Toledo, Switzerland
3.	Halogen lamp	500 W	China
4.	Oven	TMOV – 420(0-260 ^{0}C)	Gallenkamp, England.
5.	Furnace	LH120/14(30-3000 ^{0}C)	Nebertherm GmbH, Germany.
6.	High Vacuum Pump	E2M2	
7.	X – Ray Diffractometer.	Empyrel	PANalytical, Netherland
s8.	Scanning Electronic Microscopic.	Phenom pro-X	Phenomworld, Netherland
9.	Spectrophotometer.	UV – 2500S	Shimadzu, Japan
10.	pH, Conductivity, TDS metre	HI9A129	Portable hanna combo

3.2 Methods

Fig. 3.1 gives a detailed methodology of the operations involved in the synthesis, characterization and application of $ZnFe_2O_4$/α- Al_2O_3 composite photocatalysts.

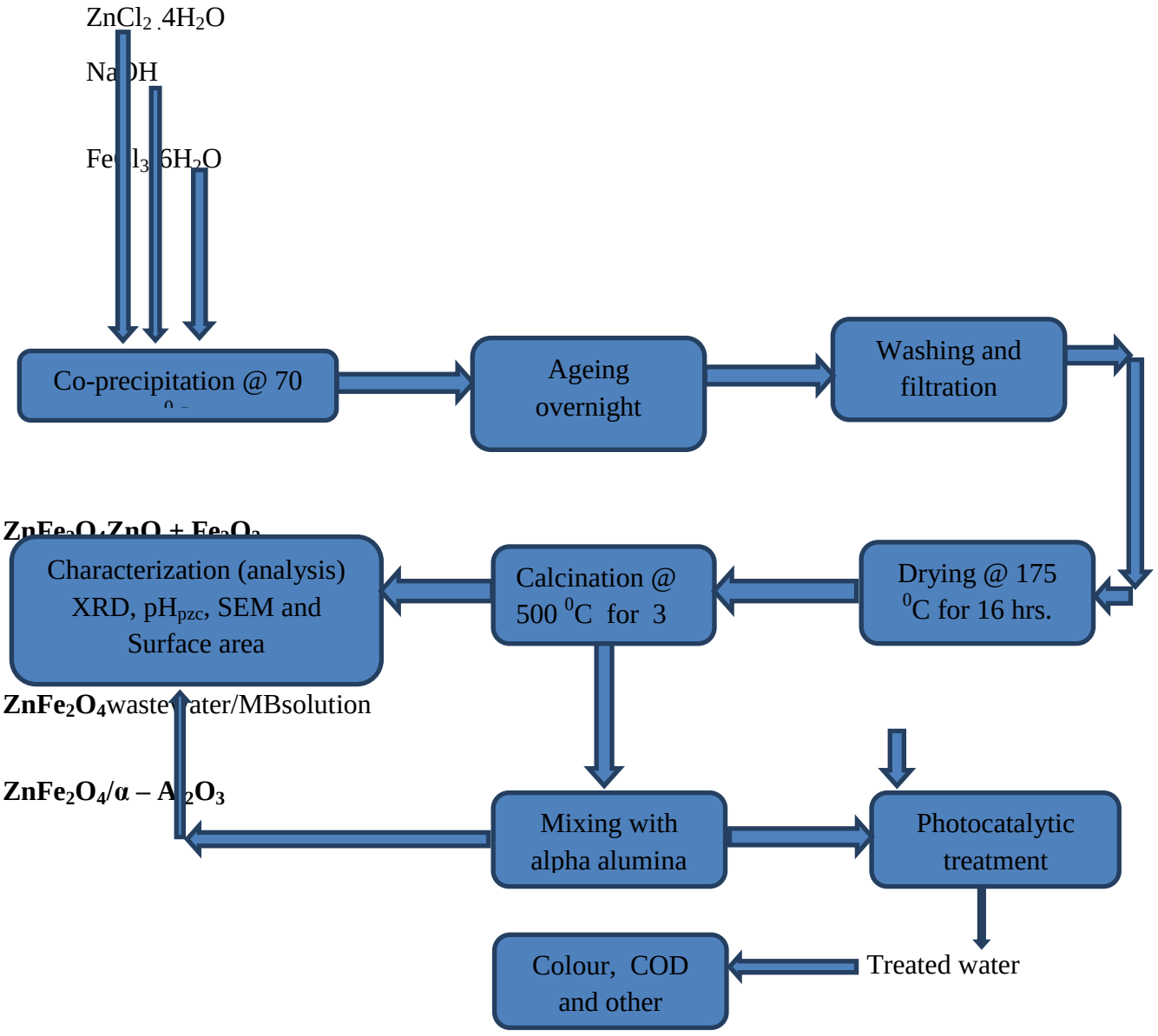


Fig. 3.1. Flow Diagram of the Research Methodology

3.2.1 Synthesis of $ZnFe_2O_4$ and $ZnFe_2O_4/Al_2O_3$

25.5 g Zinc chloride and 69 g of Iron Chloride was made with 300 ml of distilled water separately, it was then mixed in a 2000 ml conical flask with vigorous stirring at 70 ^{0}C and 70 g of diluted sodium hydroxide was added slowly at a constant rate and stirring to the mixed solution of Zinc Chloride and Iron Chloride.The precipitate formed (via eq. 3.1) was aged for 24 hrs, and then washed thoroughly for several times with distilled water to remove any trace of Sodium Hydroxide. To further remove water, the solids were vacuum filtered using a vacuum filtration pump. The solids were then calcined at 500 ^{0}C for 3 hrs, to yield $ZnFe_2O_4$ (eq. 3.2)

$$ZnCl_2 + 2FeCl_3 + 8NaOH \rightarrow Zn(OH)_2 + 2Fe(OH)_3 + 8\,NaCl \qquad (3.1)$$

$$Zn(OH)_2 + 2Fe(OH)_3 \rightarrow ZnFe_2O_4 + 4H_2O \qquad (3.2)$$

$ZnFe_2O_4$and α-Al_2O_3 in various proportions (10 wt%, 20 wt%, 30 wt% and 40 wt%)were dispersed in aqueous suspension with vigorous stirring at a temperature of 50 ^{0}C for 1 hr, to yield $ZnFe_2O_4/\alpha$-Al_2O_3 composites.

3.3 Characterization of the synthesized $ZnFe_2O_4$ and $ZnFe_2O_4/\alpha$-Al_2O_3 composites.

3.4.1 X-Ray Diffraction (XRD) Spectroscopy

Empyrel X-ray diffraction (XRD) machine was used to examine the crystal structures of the synthesized photocatalysts particles. It is a method of determining the arrangement of atoms within a crystal, in which a beam of X-rays strikes a crystal and diffracts into many specific directions using a diffractometer. It provides detailed information on the crystallographic structure and physical properties of materials and thin films.

3.4.2 SEM Analysis

Scanning electron microscopy (SEM) analysis: A Hitachi X-650 Scanning Electron Microanalyzer was used to take the micrographs of the samples, at an accelerating voltage of 10.0 kV and a working distance of 10.0 mm,. The samples were first calcined and later mounted on aluminium stubs using conductive glue and were then coated with a thin layer of carbon paste tape on copper pegs and coated with a film of evaporated gold, prior to the observation.

3.4.3 Specific surface area determination

The surface area was estimated using Sear's method by agitating 1.5 g of powdered sample in 100 ml of diluted hydrochloric acid of a pH of 3, 30 g of sodium chloride was then added with a constant stirring and the volume was made up to 150 ml with deionized water. The solution was titratred with 0.10 N NaOH and the volume needed to raise the pH from 4 to 9 was recorded. Then the surface area of synthesized phohocatalysts was estimated (Sears, 1981).

3.4.4 Determination of the pH of point of zero charge

0.1 M solution of KCl was prepared and added 25 ml of the solution and then altered its pH to the desired value by adding the concentrated HCl/NaOH (1M). 25 ml of the KCl solution were added to the labeled flask (1-11) and 0.05 g of the synthesized photocatlyst while shaking, the pH values of the solutions were taken and recorded followed by shaking the flask for 2 hrs and the pH values were recorded again after which the particles were settled (Rockafellow *et al*., 2009).

3.5 Photocatalytic experiments

3.5.1 Photocatalytic decolorization of MB solution

A 100 ml/L stock solution of MB was prepared using distilled water for all the experiments. The adsorption tests under dark condition were carried out, for the evaluation of the adsorption – desorption of MB on the surfaces of synthesized photocatalysts. 100 ml of solution of MB was taken from the stock solution and put in the reactor and kept in the dark at room temperature with continuous stirring for three and half hours. After one hour of continuous stirring in the dark, an aliquot of 5 ml was withdrawn from the reactor and then switched on the lamp to provide irradiation for the two and half hours (2:30 hrs.). 5 ml of the aliquot was withdrawn with a syringe at regular interval of time; same procedure was strictly followed for the decolourization of methyl orange.

100 ml of solution ofMBwas taken into reactor; 0.1 g of photocatalysts was added. Then the suspension was kept in the dark at room temperature with continuous stirring by the help of magnetic stirrer. After one hour in the dark, 5 ml of the suspension was taken and stored in a vail for the analysis. The suspension was then irradiated with the source of halogen lamp while stirring of the suspension was going on. An aliquot of 5 ml was taken from the reactor at regular interval of 30 mins. Then, the catalysts were filtered and the samples were then analized using a UV – Vis spectrophotometer. Same procedures were followed for composite photocatalysts that is $ZnFe_2O_4/\alpha\text{-}Al_2O_3$ of (10 wt%, 20 wt%, 30 wt%, and 40 wt%).

3.5.1 Photocatalytic degradation of MB solution

100 ml of solution of MB was taken into reactor, 0.1 g of photocatalysts ($ZnFe_2O_4$ and 30wt% $ZnFe_2O_4/\alpha$-Al_2O_3 was added. Then the suspension was kept in the dark at room temperature with continuous stirring by the help of magnetic stirrer. After one hour in the dark, the suspension was then irradiated with 500 W halogen lamp while stirring of the suspension was going on. An aliquot of 5 ml was taken from the reactor at 150 mins. Then, the catalysts were filtered and COD analysis of the sample was then carried out.

3.6 Analysis of the raw and treated water samples

3.6.1 UV- Visible spectroscopic analysis

A PC based UV-Vis spectrophotometer was used for the determination of concentration of samples as per following procedure. The system is switched on and warmed up for 30 minutes and thoroughly cleaned quartz cuvettes were used. One cuvette was filled with the reference compound and the other one with the compound whose absorbance was to be measured at λmax (maximum wavelength). To get the relationship between concentration and absorbance of the compound, a calibration curve was made. Calibration solutions are made from standard solutions of known concentration. The absorbance was plotted against known concentration of the calibration samples. These calibration curves were stored in the system itself and the concentration of the unknown sample was calculated directly from the absorbance.

3.6.2 Measurement of COD

0.4 g of H_2SO_4 was placed into refluxing flask and 20 ml of aliquot was added, then 10 ml of standard $K_2Cr_2O_7$ solution and several glass beads previously dried at 600 ^{0}C for 1 hr, 30 ml $Ag_2SO_4 – H_2SO_4$ solution was added slowly with gentle swirling, then the flask was connected to

the condenser. The blank mixture was prepared and allowed to reflux for 2 hrs, cooled and the condenser was washed with distilled water, the cooled sample was then poured into Erlenmeyer flask and diluted to 150 ml then allowed to cool to temperature and then titrated the excess dichromate with standard using 2 to 3 drops of ferroin as the indicator.

3.6.3 Measurement of pH

The electrod meter was set to pH mode and immersed into the liquid sample and the pH reading was recorded.

3.6.4 Measurement of Conductivity

The electrode meter was set to conductivity mode and immersed into the liquid sample and the conductivity of the sample was then recorded.

3.6.5 Measurement of TDS

The electrod meter was set to TDS mode and immersed into the liquid sample and the total dissolved solid of the sample was then recorded.

CHAPTER FOUR

RESULTS AND DISCUSSION

4.1. Characterization of the synthesized photocatalysts

4.1.1 XRD analysis of the synthesized Photocatalysts

The XRD pattern of the prepared $ZnFe_2O_4$ displayed in Fig. 4.1 is characterized by broad low intense peaks at Bragg angles of 31.0^0, 35.1^0, 36.1^0, 42.5^0, 57.2^0 and 62.5^0 which can be assigned to the (220), (311), (222), (400), (331), (333), (440) and (622) reflection planes of $ZnFe_2O_4$ (JCPDS card No 82 – 1049). The broad peaks are due to the low crystallinity of the prepared $ZnFe_2O_4$ at 500 ^{0}C. The calcination temperature of 500 ^{0}C was selected based on the work of Jadhav *et al*. (2010) which established that $ZnFe_2O_4$ sintered at 500 ^{0}C exhibits the highest photocatlytic activity than other $ZnFe_2O_4$ samples sintered at higher temperatures. Higher sintering temperature leads to increase in the crystal size of materials there - by decreasing their specific surface area. As a heterogeneous process, the efficiency of photocatalysis increases with increase in the specific surface area of the photocatalyst used. The XRD patterns of $\boldsymbol{\alpha}$-Al_2O_3 supported $ZnFe_2O_4$ features sharp peaks at 25.85^0, 35.41^0, 43.62^0 and 57.76^0 due to $\boldsymbol{\alpha}$-Al_2O_3 (JCPDF 75 – 1862). $ZnFe_2O_4$ are hardly seen in the XRD patterns of $\boldsymbol{\alpha}$-Al_2O_3 supported $ZnFe_2O_4$ due to low cryatallinity of the synthesized $ZnFe_2O_4$. The Bragg angles of $\boldsymbol{\alpha}$-Al_2O_3 peaks shown in fig. 4.2 did not change after loading with $ZnFe_2O_4$; hence, the crystal structures of the $\boldsymbol{\alpha}$-Al_2O_3 remain unperturbed after $ZnFe_2O_4$ loading. In fact similar trend was reported in the work of Farbodand Khademalrasool, (2011). The average particle sizes of the synthesized $ZnFe_2O_4$ and α-Al_2O_3 supported $ZnFe_2O_4$ calculated using the Debye - Scherrer equation (4.1) are listed in Table 4.1.

$$\tau = \frac{k\lambda}{\beta cos\vartheta} \qquad 4.1$$

Where τ is the particle size, λ is the wave length of the x – ray radiation (Cu K$\boldsymbol{\alpha}$ = 0.1542 nm), k is the shape factor (k = 0.94), is the line width at half maximum height and ϑ is the angular position of the maximum peak (Hou*et al*., 2009).

As could be observed from the Table 4.1, the average particle size increases with increase in the weight percent of α-Al_2O_3 supported $ZnFe_2O_4$. The surface area decreases with increase in the average particle size. Similar trend was observed in the work of An *et al*, (2011).

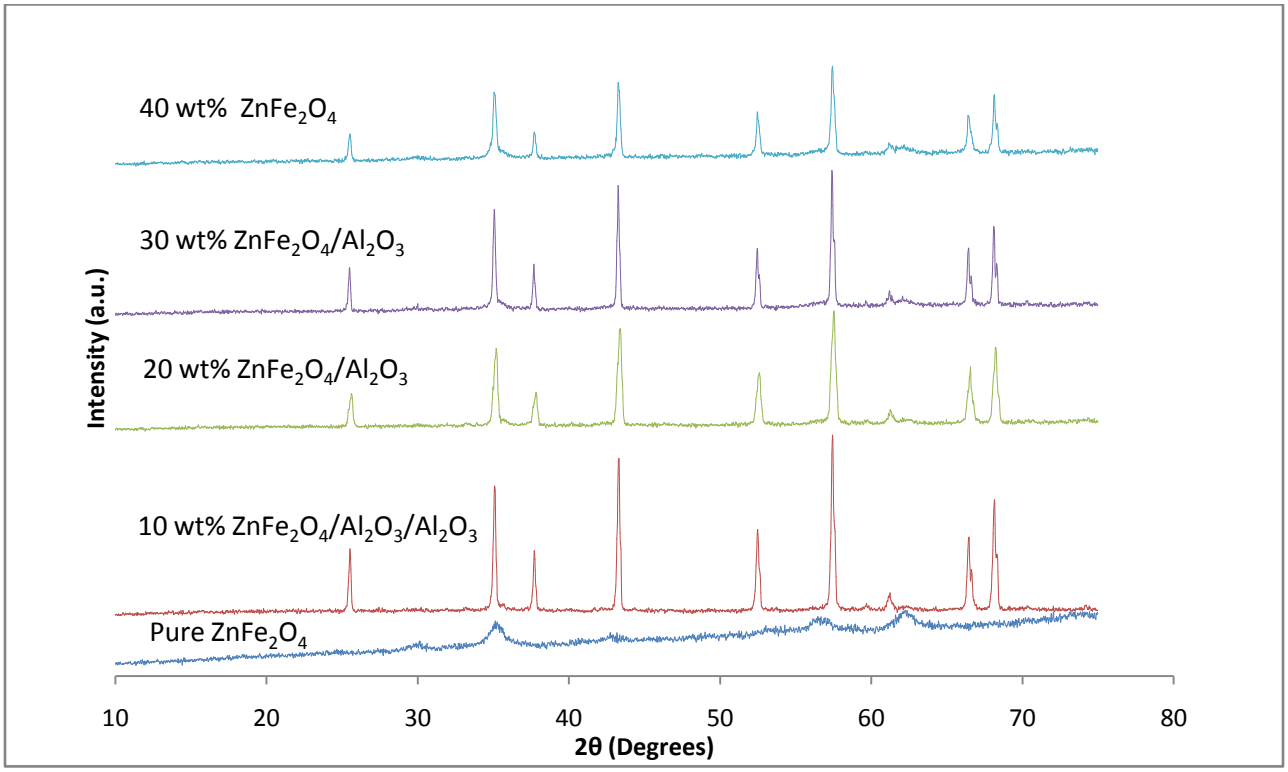


Fig. 4.1. XRD patterns of the prepared $ZnFe_2O_4$, 10 wt% $ZnFe_2O_4$/α-Al_2O_3, 20 wt% $ZnFe_2O_4$/α-Al_2O_3, 30 wt% $ZnFe_2O_4$/α-Al_2O_3 and 40 wt% $ZnFe_2O_4$/α-Al_2O_3 (ZF = ZnFe2O4 and Al = α-Al_2O_3)

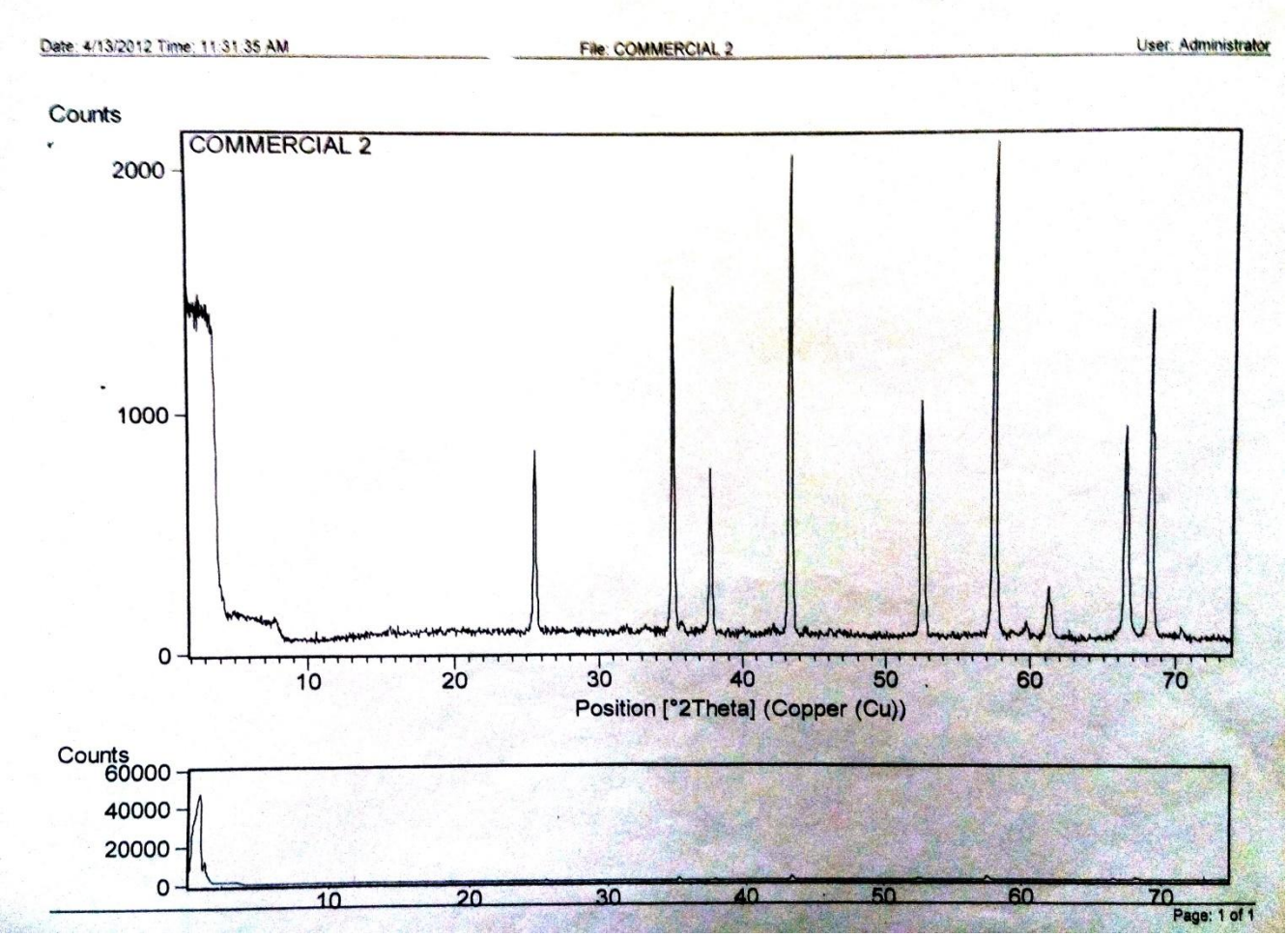


Fig. 4.2: XRD pattern of the commercial α-Al_2O_3

4.1.2. Specific Surface Areas of the Synthesized Photocatalysts

The specific surface areas of the synthesized $ZnFe_2O_4$ and α-Al_2O_3 supported $ZnFe_2O_4$ measured using the Sear's method is listed in Table 4.1. As observed from the table, the specific surface area of the unsupported $ZnFe_2O_4$ is 397 m^2/g. When $ZnFe_2O_4$ was loaded on α-Al_2O_3 the specific surface area of the materials decreased with increase in the $ZnFe_2O_4$ loading. It has been reported that the specific surface area of the photocatalysts mostly decreases with increase in the molar ratio of the active component on the support material (Kostedt *et al*., 2010).

Table 4.1. Average particle sizes and specific surface areas of the synthesized $ZnFe_2O_4$ and α-Al_2O_3 supported $ZnFe_2O_4$

Photocatalysts	Average particle size (nm)	Specific Surface Area (m^2/g)
$ZnFe_2O_4$	18.3	397
10 wt% $ZnFe_2O_4/\boldsymbol{\alpha}$-$Al_2O_3$	27.1	269
20 wt% $ZnFe_2O_4/\boldsymbol{\alpha}$-$Al_2O_3$	31.6	183
30 wt% $ZnFe_2O_4/\boldsymbol{\alpha}$-$Al_2O_3$	59.3	81
40 wt% $ZnFe_2O_4/\boldsymbol{\alpha}$-$Al_2O_3$	75.2	NA

4.1.3 Morphology of the synthesized photocatalyst.

The morphological characteristics of the synthesized $ZnFe_2O_4$ and 30 wt% $ZnFe_2O_4/\boldsymbol{\alpha}$-$Al_2O_3$ were investigated by SEM analysis. The SEM image of $ZnFe_2O_4$ sample displayed in Fig. 4.3a shows that $ZnFe_2O_4$ exhibits a compact arrangement of nanoparticles with roughly irregular shape. Most of the particles are aggregated which makes it difficult to determine the exact size

and shape of the particle (Kim *et al*, 2010). The SEM image of 30 wt% $ZnFe_2O_4/\boldsymbol{\alpha}$-$Al_2O_3$ presentedin Fig. 4.2b, reveals that the $\boldsymbol{\alpha}$-Al_2O_3 exhibits a plate/disk - like shape and $ZnFe_2O_4$ is deposited on its surface α-Al_2O_3 is more crystalline than $ZnFe_2O_4$ in good agreement with their XRD patterns of Fig. 4.1.

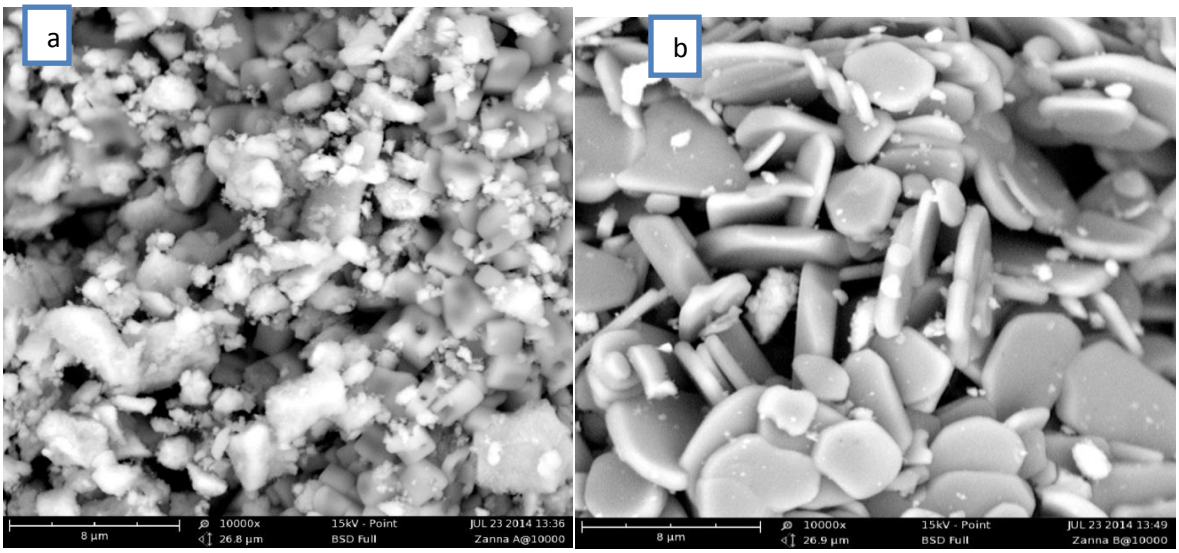


Fig. 4.3: SEM image of (a) Pure $ZnFe_2O_4$ and (b) $ZnFe_2O_4$/α-Al_2O_3 composite.

4.1.4. pH at zero of point charge of the photocatalyst

The pH values of different wastewaters are different and they influence the photocatalytic reactions for removal of the pollutants (Rosales *et al*., 2007). pH at point of zero charge (pH_{PZC}) determines the pH where the surface charge of a material is zero or neutral. It is very important to know the pH_{pzc} of the synthesized photocatalysts. The pH_{pzc} of the synthesized photocatalysts are shown in Table 4.2. The measured pH at point of zero charge of synthesized $ZnFe_2O_4$ via co - precipitation method is 7.5, which is close to the values of 7.6 - 8 reported in the literature (Rockafellow *et al.*, 2009). The difference in the value might be attributed to the method of preparation. Above this pH_{PZC} (7.5), the $ZnFe_2O_4$ surface is negatively charged due to the formation of O^{2-} on the surface while below 7.5 the surface charge of $ZnFe_2O_4$ particles are

positively charged as a result of formation of Zn^{2+}.For the $ZnFe_2O_4/Al_2O_3$ composites.it was observed that the values increased from 10 wt% $ZnFe_2O_4/Al_2O_3$ to 20 wt% $ZnFe_2O_4/Al_2O_3$and decreases at the wt% of 30 and 40. Hence, the presence of Al_2O_3 has a great effect or effluence on altering the pH_{PZC} of $ZnFe_2O_4$ (Dong *et al.,* 2015).

Table 4.2.pH at point of zero charge of the photocatalysts

Photocatalysts	pH_{pzc}
$ZnFe_2O_4$	7.5
10 wt% $ZnFe_2O_4/\alpha$-Al_2O_3	7.8
20 wt% $ZnFe_2O_4/\alpha$-Al_2O_3	8.3
30 wt% $ZnFe_2O_4/\alpha$-Al_2O_3	8.1
40 wt% $ZnFe_2O_4/\alpha$-Al_2O_3	7.9

4.2. Photocatalytic decolourization of MB using the synthesized photocatalyst

The photocatalytic activity of the prepared photocatalysts was first evaluated using MB dye as a model substrate. MB is widely used dye and is often found in textile effluents. MB is also used as test molecule for evaluating the activity of series of photocatalyst (Disanto *et al.,* 1972). The effects of varying $ZnFe_2O_4$ loading (10, 20, 30 and 40 wt%) on α-Al_2O_3 support were investigated at an initial MB concentration of 50 mgl^{-1} with a photocatalyst dosage of 1.0 gl^{-1}. It is clearly seen from Fig.4.4 that the percentage photocatalytic degradation of MB increases with increase in the $ZnFe_2O_4$ loading from 10 wt% to 30 wt% due to the increase in the number of $ZnFe_2O_4$ active sites because photocatalytic degradation occurs at the active sites. However,

percentage photocatalytic degradation of MBdecreased when $ZnFe_2O_4$ loading was increased to 40 wt%. The significant reduction of the photocatalytic activity of the sample containing 40 wt % $ZnFe_2O_4$ can be attributed to the increased agglomeration of $ZnFe_2O_4$ particles on α-Al_2O_3, thereby decreasing the rate of diffusion of photogenerated electron-hole pairs onto the MB molecules at the interface of solid photocatalyst- MB solution. Retardation of the diffusion of electron-hole pairs decreases the extent of photocatalytic degradation (Li *et al*., 2011). Agglomeration of $ZnFe_2O_4$ particles on the surface of α-Al_2O_3 decreases the specific surface area and light penetration for an efficient photocatalytic degradation. Similar observations were reported for photocatalytic degradation of methyl orange and Orange II dyes on supported α-Fe_2O_3 photocatalysts. Thus, 5 wt% α-Fe_2O_3/zeolite-HY exhibited the highest activity for degradation of methyl orange (Jaafar *et al*., 2013), and 25 wt % Fe_2O_3/alumina exhibited the highest activity for degradation of Orange II dye (Li *et al*., 2011). In the present work, highest photocatalytic degradation of MB was achieved with 30 wt % $ZnFe_2O_4$/α-Al_2O_3. As can be seen from Fig.3, the photocatalytic activity of the unsupported $ZnFe_2O_4$ is higher than those of 10 wt % $ZnFe_2O_4$/α-Al_2O_3 and 40 wt % $ZnFe_2O_4$/α-Al_2O_3, but lower than those of 20 wt % $ZnFe_2O_4$/α-Al_2O_3 and 30 wt % $ZnFe_2O_4$/α-Al_2O_3. Therefore, the best loading of $ZnFe_2O_4$ on the α-Al_2O_3 support is a tradeoff between good dispersion of $ZnFe_2O_4$ on the support and the amount of the photocatalytically active sites. Moreover, Fu *et al*., (2010) reported that Al_2O_3 support improves the formation of OH radicals by photocatalysts.

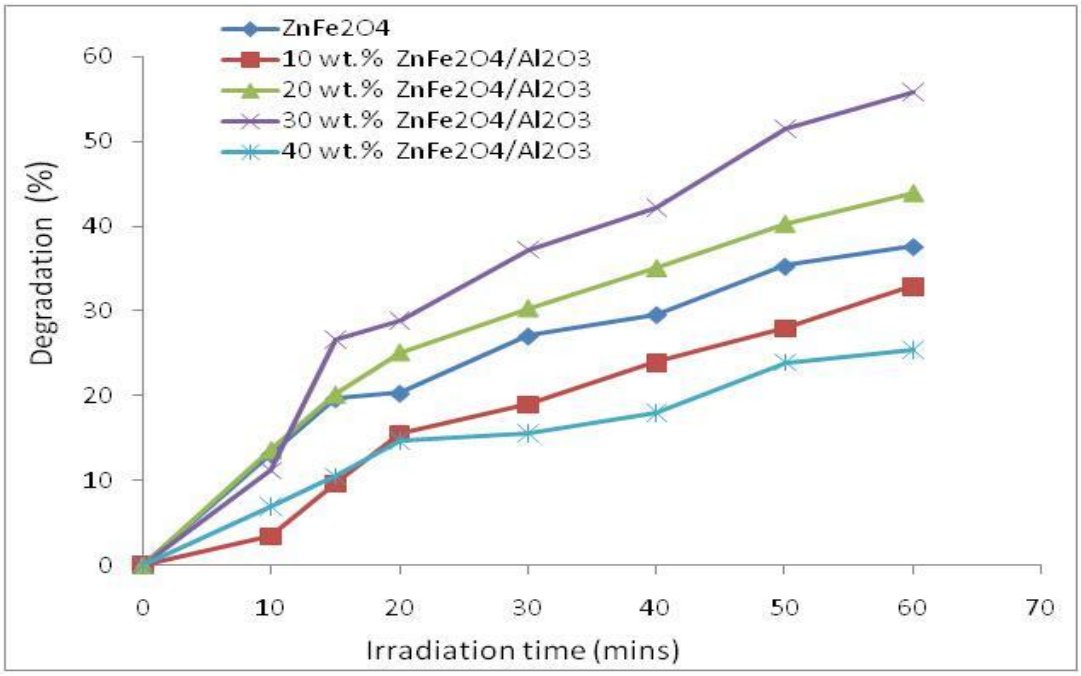


Fig. 4.4. Photocatalytic degradation of MB using $ZnFe_2O_4$ and α-Al_2O_3 supported Z_2nFeO_4

The effect of the initial MB concentration on its photocatalytic degradation using 30 wt % $ZnFe_2O_4$/α-Al_2O_3 was investigated by varying MB concentration from 25 to 100 mgl^{-1}. Fig.4.5, shows that the photocatalytic degradation decreased with increasing initial concentration of MB. For instance, when the initial concentration of MB was increased from 25 to 100 mgl^{-1}, the photocatalytic degradation decreased from 68 % to 22 %,after 60 min of visible light irradiation. This observation can be explained as follows: the generation of electrons and holes is the same for a given dosage of photocatalyst and intensity of the incident radiation. At higher initial concentrations, MB molecules can absorb some of the incident radiation. This will decrease the amount of available light photons that will drive the photocatalytic process (Jaafar *et al*., 2012).

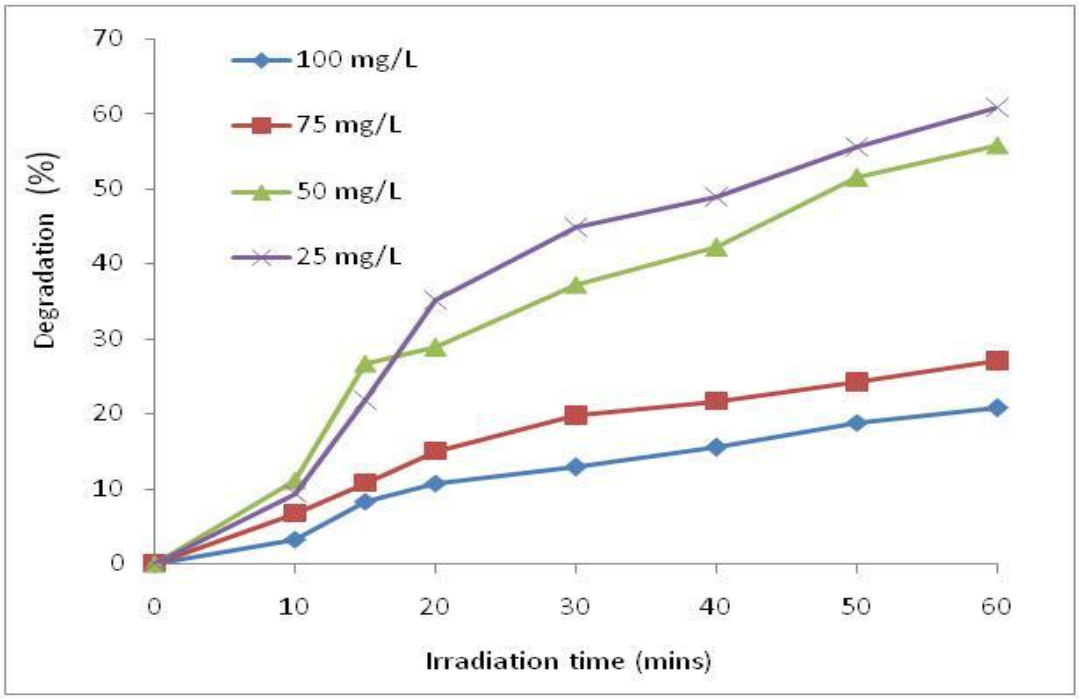


Fig. 4.5 Effect of initial concentration of MB on its photocatalytic degradation using 30 wt % $ZnFe_2O_4/\alpha\text{-}Al_2O_3$

As shown in Fig.4.6, the kinetic data nicely fitted the Langmuir–Hinshelwood kinetic model with R^2 of 0.970. The calculated values of k_r and K_e are 0.005 $mgl^{-1}min^{-1}$ and 0.111 lmg^{-1}, respectively. The kinetic data can used for the design of photocataltic reactors that utilize α-Al_2O_3 supported $ZnFe_2O_4$ as the photocatalyst.

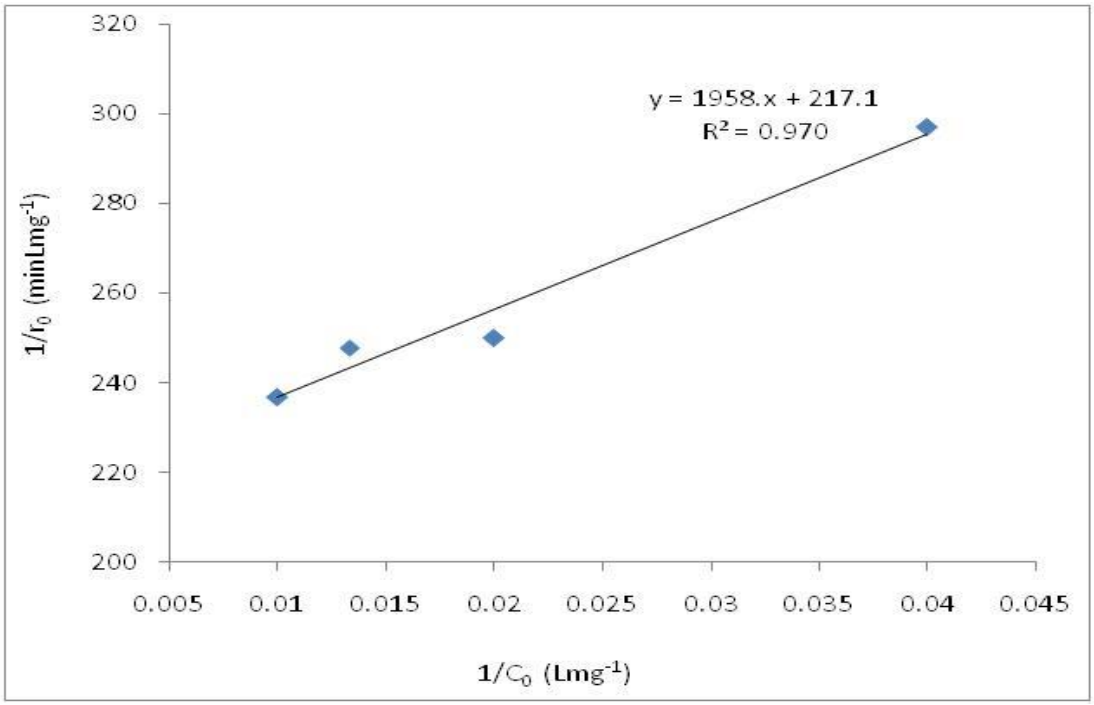


Fig. 4.6 Langmuir–Hinshelwood kinetic plot for the photocatalytic degradation of MB using 30wt % $ZnFe_2O_4/\alpha\text{-}Al_2O_3$

4.3 Photocatalytic treatment of textile effluent

The properties of the raw treated textile effluent used in the work are presented in Table. 4.3. Also presented in the Table are the properties of the treated textile effluent via photolysis and photocatalysis with $ZnFe_2O_4$ and 30 wt% $ZnFe_2O_4/\alpha\text{-}Al_2O_3$.Due to the complex nature of most industrial effluents, the organic content of the effluents is measured using lump parameters such as Chemical oxygen Demand (COD), Biological Oxygen Demand (BOD) and Total Ogarnic Carbon (TOC) etc. Conductivity and TDS indirectly measure the amount of inorganic species (such as dissolved salts) in the effluent. As seen in Table 4.3., upon photolysis of the effluent, smaller changes were observed in the properties of the effluent when compared with photocatalysis. This observation can be attributed to more efficient degradation of the organic and inorganic pollutants present in the effluent via photocatalysis. The deacrease in the effluent's pH is due to to the release of CO_2 during photocatalytic degradation of organic pollutants. The

observed reduction of the effluent's conductivity and TDS can be attributed to photocatalytic decomposition of inorganic and organometallic dyes and other pollutants.

Table 4.3. Properties of the raw and treated textile effluent

	pH	Conductivity (mg/L)	TDS(µs/cm)	COD (mg/L)
Raw effluent	8.65	1966	982	784
Effluent treated via photolysis	8.61	1940	974	688
Effluent treated via photocatalysis with $ZnFe_2O_4$	8.49	1928	965	576
Effluent treated via photocatalysis with 30 wt% $ZnFe_2O_4/\alpha\text{-}Al_2O_3$	8.23	1894	949	416

4.4.1. Photocatalytic decolourization of textile effluent

UV–vis analysis of the treated effluent provides information about the decolourization of the wastewater caused by photolytic and photocatalytic destruction of the chromophores responsible for the colour of the wastewater (Boorman *et al*.,1999). The results of decolourization of textile effluent are presented in Fig 4.7. Irradiation of the textile effluent in the absence of photocatalyst (Photolysis) resulted in the removal of only 15% of the effluent's initial colour after 90 mins. When decolourization of the textile effluent via photocatalytic treatment under visible light was performed, percentage decolourization of 30% and 49% were observed for $ZnFe_2O_4$ and 30 wt% $ZnFe_2O_4/\alpha\text{-}Al_2O_3$ respectively. Thus, 30 wt% $ZnFe_2O_4/\alpha\text{-}Al_2O_3$ is more effective in colour removal than the $ZnFe_2O_4$. This higher adsorption efficiency of 30 wt% $ZnFe_2O_4$ on α -

Al_2O_3can be attributed to the formation of more OH radicals in the presence of Al_2O_3 support as repoted by Fu *et al*., (2010).

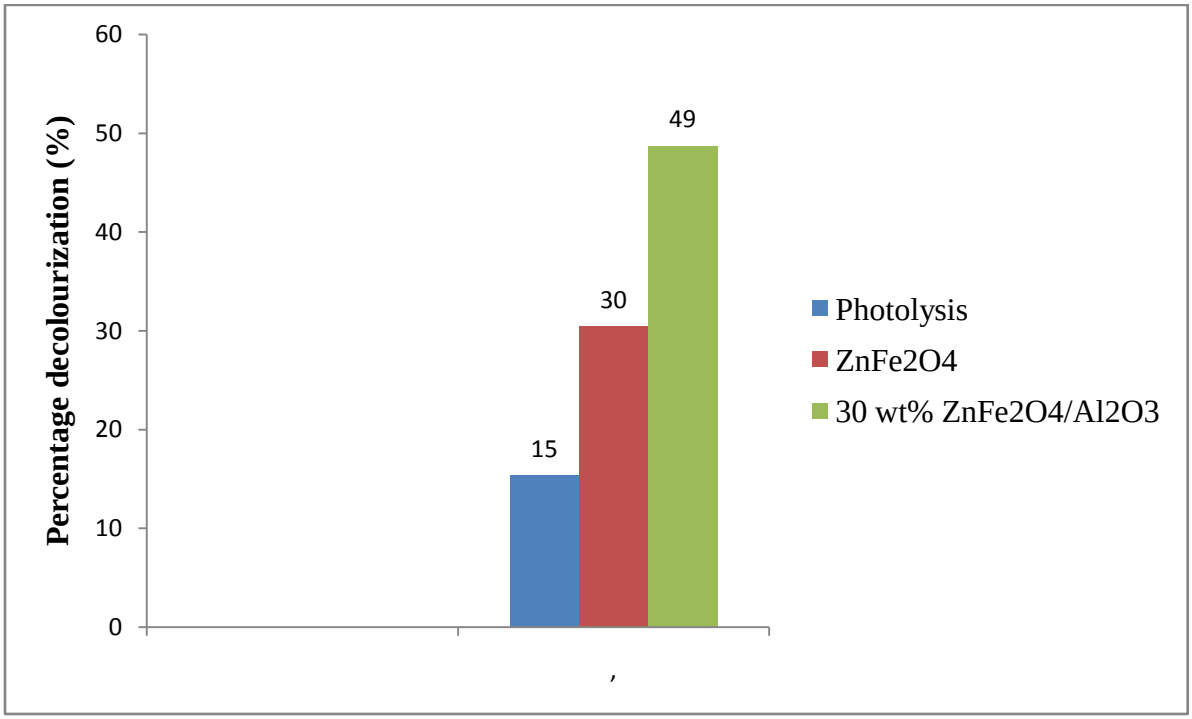


Fig. 4.7Decolourization of textile effluent via photolysis and photocatalysis using $ZnFe_2O_4$ and 30 wt% $ZnFe_2O_4/\alpha$-Al_2O_3. [Irradiation time - 90 mins. photocatalyst dose - 0.1 g/L]

4.4.2 Photocatalytic degradation of textile effluent

The results of COD removal from textile effluent via photolysis and photocatalysis are presented in Fig. 4.8. It was found that irradiation of textile effluent for 90 mins in the absence of photocatalysts (photolysis) resulted in the COD removal of only 10 – 11%, this indicates that the organic load of the sample irradiated without photocatalyst did not change much, and the small COD removal observed was due to the photochemical oxidation of the organic compounds present in the textile effluent (Pelentridou *et al.*, 2009). Therefore, irradiation without photocatalyst is not sufficient to efficiently degrade the textile effluent. When the solution was

exposed to visible light irradiation in the presence of $ZnFe_2O_4$ and 30 wt% $ZnFe_2O_4/\alpha$-Al_2O_3 for 90 mins, 27% and 47% COD removal was achieved, respectively. This evidently shows that 30 wt% $ZnFe_2O_4/\alpha$ - Al_2O_3 has better photocatalytic performance than the bare $ZnFe_2O_4$ for the treatment of the textile effluent.

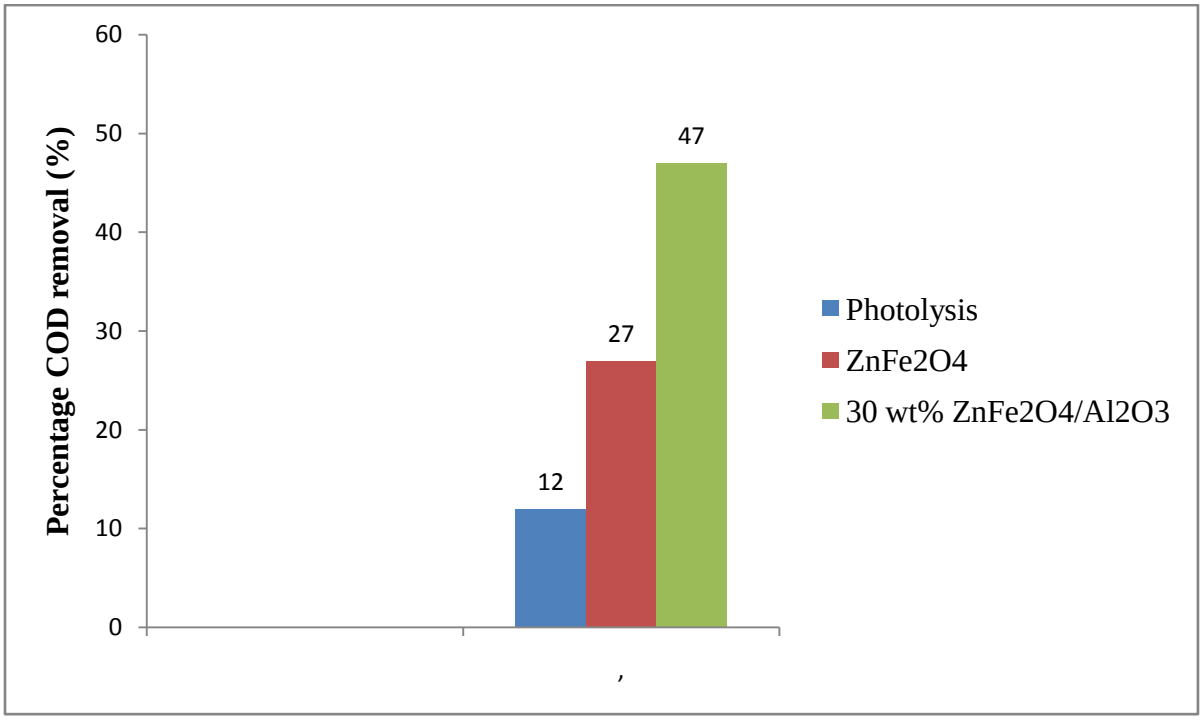


Fig. 4.8.COD removal from textile effluent via photolysis and photocatalysis using $ZnFe_2O_4$ and 30 wt% $ZnFe_2O_4/\alpha$-Al_2O_3. [Irradiation time - 90 mins. photocatalyst dose - 0.1 g/L]

CHAPTER FIVE

CONCLUSIONS AND RECOMMENDATIONS

5.1 Conclusions

From the results and discussion presented in the previous chapter, the following conclusions were drwan:

1. The prepared $ZnFe_2O_4$ is characterized by low crystallinity. The size of $ZnFe_2O_4$ particles is smaller than that of the α-Al_2O_3 support. The specific surface area of the α-Al_2O_3 supported $ZnFe_2O_4$ photocatalysts decreases with increase in the $ZnFe_2O_4$ loading.
2. The percentage degradation of MB increased with increase in the $ZnFe_2O_4$ loading from 10 wt% to 30 wt% and decreased when the loading was raised to 40 wt%. The photocatalytic activity of 30 wt % $ZnFe_2O_4$/α-Al_2O_3 is higher than those of $ZnFe_2O_4$ and other α-Al_2O_3 supported photocatalysts containing 10 wt%, 20 wt% and 40 wt% of $ZnFe_2O_4$.
3. α-Al_2O_3 support improves the photocatalytic activity of $ZnFe_2O_4$ under visible light irradiation, and the optimum loading of $ZnFe_2O_4$ on α-Al_2O_3 is 30 wt %.
4. Analysis of the kinetic data for the photocatalytic degradation of MB using the Langmuir–Hinshelwood kinetic model yielded 0.005 $mgL^{-1}min^{-1}$ for the intrinsic photocatalytic reaction rate constant and 0.111 Lmg^{-1} for the adsorption equilibrium constant.
5. Photocatalytic treatment of real textile effluent resulted in more effective (when compared to photolytic treatment) in the reduction of effluent's colour, COD, pH, conductivity and TDS.

6. 30 wt% $ZnFe_2O_4/Al_2O_3$ was found to be more effective than bare $ZnFe_2O_4$ for the reduction of effluent's colour, COD, pH, conductivity and TDS.

5.2 Recommendations

Furtherance to the present study, the following recommendations have been made:

1. More research is needed to establish the mechanism of photocatalytic treatment of textile effluents with 30 wt% $ZnFe_2O_4/Al_2O_3$,and also to optimize the factors affecting photocatalytic treatment of textile effluent.
2. Pilot plant photocatalytic wastewater treatment plants that utilize the synthesized photocatalysts should be developed.
3. The synthesized photocatalysts are found to be active under visible light irradiation; hence, they can be used for harnessing solar energy to drive chemical processes.

REFERENCES

Adin, A., Asano, T. (1996).*The Role of Physical-chemical treatment in wastewater reclamation and reuse.*Journal of Water Science Technology, 37: 79-90.

Al-Kdasi, A., Idris, A., Saed, K. and Teong Guan, C. (2004).*Treatment of Textile Wastewater by Advanced Oxidation Processes.*A reviewJournal of Global Nest, 6: 222-230.

Amadelli, R., Samiolo, L., Maldotti, A., Molinari, A., Valigi, M., and Gazzoli, D. (2008).*Preparation, characterisation, and photocatalytic behaviour of Co-TiO2 with visible light response.*International Journal of Photoenergy. 2008: Article ID 853753

An, T.C., An, J.B., Yang, H., Li, G.Y., Feng, H.X., Nie, X.P. *(*2011). *Photocatalytic degradation kinetics and mechanism of antivirus drug-lamivudine in TiO2 dispersion.*Journal of Hazardous Material, *197*: 229–236.

Arya. D., Kohli, P. (2009). *Environmental Impact of Textile Wet Processing,* Pollution control house, Delhi, India.

Atif, S. (2002).*Impact of Environmental Regulations on the Textile Sector of Pakistan, Geneva.*Journal Environmental Health Perspectives,107: 220-229.

Babu R, Parande A, Raghu S, Kumar T (2007).*Textile Technology - Cotton Textile Processing: Waste Generation and Effluent Treatment.* Journal of Cotton Science,11:141-153.

Bach, U., Lupo, D., Comte, P., Moser, J.E., Rtel, F.W., Salbeck, J., Spreitzer, H., Grätzel, M. *(*1998). *Solid-state dye-sensitized mesoporous TiO_2 solar cells with high photon-to-electron conversion efficiencies.*Nature,395: 583–585.

Barclay, S., Buckley, C. (2000).*Waste Minimisation Guide for the Textile Industry: A Step towards cleaner production.* The pollution research group, univ of Natal, Durban, South Africa.

Benabbou, A.K., Derriche, Z., Felix, C., Lejeune, P. and Guillard, C. (2007). Photocatalytic inactivation of Escherischia coli: *Effect of concentration of TiO_2 and microorganism, nature, and intensity of UV irradiation.* Journal of Applied Catalysis B: Environmental,76: 257-263.

Boorman, G.A., Dellarco, V., Dunnick, J.K., Chapin, R.E., Hunter, S., Hauchman, F., Gardner, H., Cox, M. and Sills, R.C. (1999). *Drinking Water Disinfection Byproducts: Review and Approach to Toxicity Evaluation.* Journal Environmental Health Perspectives,107: 207-217.

Boumaza, S., Boudjemaa, A., Bouguelia, A., Bouarab, M., Trari. (2010). *Visible light induced hydrogen evolution on new hetero-system $ZnFe_2O_4/SrTiO_3$. Journal of Appl. Energy.* 87: 2230–2236.

Cao, X., Gu, L., Lan, X., Zhao, C., Yao, D. and Sheng, W. (2007). *Spinel ZnFe2O4 nanoplates embedded with Ag clusters: preparation, characterization, and photocatalytic application.* Journal of Material Chemistry and Physics, 106: 175–180

Chen, D., Hou, J., Yao, L., Jin, H., Qian, G. and Xu, Z.P. (2010).*Ferrite materials prepared from two industrial wastes: electroplating sludge and spent pickle liquor*. Journal of Seperation and Purification Technology, 75: 210–217.

Chen, C., Liang, Y. and Zhang, W. (2009).*$ZnFe_2O_4$/MWCNTs composite with enhanced photocatalytic activity under visible-light irradiation*, Journal of Alloy Compound, 501: 168–172.

Chen, X., Shen, Z., Zhu, X., Fan, Y., Wang, W. (1996).*Advanced Treatment of Textile Wastewater for Reuse Using Electrochemical Oxidation and Membrane Filtration.*Chinese Academy of Science.

Cheng, P., Li, W., Zhou, T., Jin, Y. and Gu, M. (2004). *Physical and photocatalytic properties of zinc ferrite doped Titania under visible light irradiation,* Journal of Photochemistry andphotobiology, A, 168: 97–101.

Daneshvar, N., Aber, S., Dorraji, M.S.S., Khataee, A.R. and Rasoulifard, M.H. (2007). *Photocatalytic degradation of the insecticide diazinon in the presence of prepared nanocrystalline ZnO powders under irradiation of UV-C light.*Journal of Separation and Purification Technology, 58: 91-98

Das, (2000).*Recent progress in environmental catalytic technology," Catalysis Surveys from Japan,* 4: 83–90.

Disanto, A.R., Wagner, J.G. (1972). *Pharmacokinetics of highly ionized drugs. II. Methylene blue absorption, metabolism, and excretion in man and dog after oral administration.* Journal of Pharmaceutical Science, 61: 1086-1090.

DOE (Department of Environment), (2008).*Guide for Assessment of Effluent Treatment Plants EMP/EIA Reports for Textile Industries.*Ministry of Environment and Forest, Bangladesh.

Dom, R., Subasri, R., Radha, K. and Borse, P.H. (2011).*Synthesis of solar active nanocrystalline ferrite, MFe_2O_4 (M: Ca, Zn, mg) photocatalyst by microwave irradiation.* Journal of Solid State Community, 151: 470 – 473.

Dong, H., Zeng, G., Tang, L., Changzheng, F., Zhang, C., He, X. and He, Y. (2015). *An overview on limitations of TiO_2 – based particles for photocatalytic degradation of organic pollutants and the corresponding countermeasures.* Water Research,79 : 128 – 146.

Dutta, F., Rahman, M.A., Qamar, M., Muneer, M., Bahnemenn, D. (2014).*Semicondcutor mediated photocatalysed degradation of a pesticide derivative, acephate in aqueous suspensions of titanium dioxide. Journal of Advance .Oxidation Technol,* 9: 103-109.

Ehrhardt, H., Campbell, SJ. and Hofmann, M. (2003). Journal of Screen materials, 48: 1141.

Emeline, A.V.; Ryabchuk, V.K.; Serpone, N. (2005).*Dogmas and misconceptions in heterogeneous photocatalysis. Some enlightened reflections.*Journal of Phys. Chem. B, *109*: 18515–18521.

EPA, (2002).*Wastewater technology fact sheet: Aerated, partial Mix Lagoons.* United States Environmental protection agency.EPA 832-F-02-008.

Eswaramoorthi, S., Dhanapal, K., Chauhan, D. (2008).*Advanced in Textile Waste Water Treatment: The Case for UV-Ozonation and Membrane Bioreactor for Common Effluent Treatment Plants.*Coimbatore, India.

Etter, B1., Tilley, E., Khadka, R., and Udert, K.M. (2011). *Low-cost struvite production using source-separated urine in Nepal.*Journal of Water Resource,45: 852-862.

Faber, P., Ronald, A., and Millar, B.W. (2005). *Methylthioninium chloride: pharmacology and clinical applications with special emphasis on nitric oxide mediated vasodilatory shock during cardiopulmonary bypass.* Anaesthesia, 60: 575-587.

Farbod, M., Khademalrasool, M. *(*2011).*Synthesis of TiO2 nanoparticles by a combined sol-gel ball milling method and investigation of nanoparticle size effect on their photocatalytic activities.*Powder Technology,214: 344–348.

Fetiera, A. (2009). Journal of American Ceramic Society, 92: 967.

Fu, Y., Chang, W., Wang, H. and Liu, C. (2010). *Synthesis and characterization of anatase TiO_2 nanolayer coating on Ni–Cu–Zn ferrite powders for magnetic photocatalyst,* Journal of Material Resources., 25: 134–140.

Fujishima, A., Rao, T.N. and Tryk, D.A. (2000).*Titanium dioxide photocatalysis.*Journal of Photochemistry and Photobiology C: Photochemistry Reviews, 1: 1-21.

Georgiou, D., Aivazidis, A., Hatiras, J., and Gimouhopoulos, K. (2003).*Treatment of cotton textile wastewater using lime and ferrous sulfate.*Journal Water Resources, 37: 2248-2250.

Hameed, B.H., Hasssan, H., (2009). *Fe – clay as effective heterogeneous fenton catalyst for the decolorization of reactive Blue 4.*Journal of chemical engineering, 171: 912-918.

Hamidin, N., Yu, Q.J. and Connell, D.W. (2008).*Human health risk assessment of chlorinated disinfection by-products in drinking water using a probabilistic approach.*Journal Water Resource, 42: 3263-3274.

Hoffmann, M.R., Martin, S.T., Choi, W. and Bahnemann, D.W. (1995).*Environmental Applications of Semiconductor Photocatalysis.*Journal of Chemical Reviews,95: 69-96.

Hou, X., Feng, J., Xu, X. and Zhang, M. (2009).*Synthesis and characterizations of spinel $MnFe_2O_4$ nanorod by seed-hydrothermal route.*Journal of Alloy Compound, 491: 258–263.

Hrudey, S.E. (2009). *Chlorination disinfection by-products, public health risk tradeoffs and me.* Journal Water Research,43: 2057-2092.

Jaafar, N.F., Jalil, A.A. Triwahyono, S., Muhid, M.N.M. Sapawe, N., Safar, M.A.H, Asaari, H. (2012). *Photodecolorization of Methyl Orange over α- Fe_2O_3- supported HY catalysts,*

the effect of catalyst preparation and dealumination. Journal of Chemical Engineering, 191: 112-122.

Jadhav, S.D., Hankare, P.P., Patil, R.P. and Sasikala, R. (2010).*Effect of sintering on photocatalytic degradation of methyl orange using zinc ferrite.*Journal of Material Letter, 65: 371–373.

Jumeri, F.A., Lin, H.N., Ariffin, S.N., Huang, N.M., TeO, P.S. (2014).*Microwave synthesis of magnetically seperable $ZnFe_2O_4$ – reduced grapheme oxide for wastewater treatment*.Journal of ceramic international.40: 7057 – 7065.

Jurenka, B. (2010). *Electrodialysis (ED) and Electrodialysis Reversal (EDR).U.D. Department of the Interior Bureau of Reclamation*.

Kaneva, N.V. and Dushkin, C.D. (2011).*Tuning of the UV photocatalytic activity of ZnO using zinc ferrite(III): powders and thin films prepared of powders.*Journal ofColloids Surface. A, 382: 211–218.

Kannan, M., Gobalakrishnan, M., Kumaravel, S., Nithyanadan, R., and Rajashankar, K. (2006).*Influence of cationization of cotton on reactive dyeing.* Dept of Textile Tech, PSG college of Tech, Coiambatore, Tamilnadu, India.

Karos, A., (2013). *Process water treatment by electrolytic processes.*Fraunhofer Institute for Interfacial Engineering and Biotechnology.

Kim, T.Y., Lee, Y., Park, K., Kim, S.J. and Cho, S.Y. (2010).*A study of photocatalysis of TiO_2 coated onto chitosan beads and activated carbon.* Research on Chemical Interface, 31: 343-358.

Kim, H.G., Borse, P.H., Choi, W. and Lee, J.S. (2005).*Photocatalytic nanodiodes for visiblelight Photocatalysis.Journal* Chemical Interface,44: 4585–4589.

Kiriakidou, F., Kondarides, D., Verykios, X. (1999).*The Effect of operational parameters and TiO_2 – Doping on the photocatalytic degradation of azo-dyes.Journal* Catalysis Today, 54:119-130.

Klimkiewicz, R., Wolska, J., Preepiera, A., prezpiera K., Jablonski, M. and Lenart S. (2009). Journal of masterial resource Bull, 44: 15 - 20

Kostedt IV, W.L., Drwiega, J., Mazyck, D.W., Lee, S., Sigmund, W., Wu, C. and Chadik, P. (2005).*Magnetically agitated photocatalytic reactor for photocatalytic oxidation of aqueous phase organic pollutants.*Journal of Environmental. Science Technology, 39: 8052–8056.

Kostedt IV, W.L., Byrne, H.E. and Mazyck, D.W. (2010).*A high surface area magnetic photocatalyst with controlled pore size.*Journal of Environmental and Sustainable Energy, 29: 10–16.

Lafond, R. (2008). *Moving Bed Biofilm Reactor (MBBR) A Compact technology for upgrading Canadian municipal aerated Lagoons,* Business Development and Marketing.

Laxman, M. (2009).*Pollution and its Control in Textile Industry,* India.

Li, G.Z., Park, S., Kang, D.W., Krajmalnik-Brown, R. and Rittmann, B.E. *(*2011). *2,4,5-trichlorophenol degradation using a novel TiO_2-coated biofilm carrier: Roles of adsorption, photocatalysis, and biodegradation.* Journal of Environmental Science Technology,45: 8359–8367.

Lima, R., Bazo, A., Salvadori, D., Rech, C. and Oliveira, D. (2007).*Mutagenic and carcinogenic potential of a Textile azo dye processing plant effluent that impacts a drinking water source. Mutation research/genetic Toxicology and Environmental Mutagenesis* 626: 53-60.

Lin, Y., Ferronato, C., Deng, N., Wu, F. and Chovelon, J.-M.*(*2009). *Photocatalytic degradation of methylparaben by TiO2: Multivariable experimental design and mechanism.* Journal of Applied Catalysis. B, *88:* 32–41.

Liu, Z., Zhao, Z., and Miyauchi, M. (2009).*Efficient visible light active $CaFe_2O_4/WO_3$ based composite photocatalysts: effect of interfacial modification,* Journal of Physics and Chemistry. C, 113: 17132 – 17137.

Liu, Z. and Miyauchi, M. (2011).*Visible-light induced superhydrophilicity on a $WO_3/ITO/CaFe_2O_4$ heterojunction, Thin Film.* Journal of Chemical Community, Cambridge, UK, 2002 – 2004.

Ljubas, D. (2005). *Solar photocatalysis—a possible step in drinking water treatment.* Journal of Energy, 30: 1699–1710.

Manova, E., Tsoncheva, T., Paneva, D., Popova, M., Velinov, N., Kunev, B., Tenchev, K. and Mitov, I. (2011).*Nanosized copper ferrite materials: mechanochemical synthesis and characterization.* Journal of Solid State Chemistry,184: 1153– 1158.

Marcucci, M., Ciardelli, G., Matteucci, A., Ranieri, L. and Russo, M. (2002). *Experimental Campaigns on Textile Wastewater For Reuse by Means of Different Membrane Processes.* Journal of Elsevier Science 149: 137-143.

Mittal, A. (2011).*Heterogeneous photocatalysed reaction of three selected pesticide derivatives, propham, propachlor and tebuthiuron in aqueous suspensions of titanium dioxide.*Journal of Chemosphere, 61: 457–468.

Moustafa, S. (2008).*Environmental Impacts of Textile Industries.Process Analysis of textile Manufacturing.*UNESCO-IHE, Delft, Netherlands.

Morikawa, Y., Shiomi, K., Ishihara, Y. and Matsuura, N. (1997).*Triple primary cancers involving kidney, urinary bladder, and liver in a dye worker.* American Journal of Industrial Media, 31: 44-49.

Nagaveni, K., Sinalingam, G. and Hegde, M.S. (2005). Industrial Engineering and Chemical Resource, 42: 687.

NESC, (2003).*National Environment Services Center*.

Nese, T., Sivri, N. and Toroz, I., (2007).*Pollutants of Textile industry wastewater and assessment of its discharge limits by water quality standards.*Turkish Journal.7:97- 103.

Nilsson, R., Nordlinder, R., Wass, U., Meding, B. and Belin, L. (1993).*Asthma, rhinitis, and dermatitis in workers exposed to reactive dyes.* Journal of Industrial Medicine,50: 65-70.

NODPR (National Onsite Demonstration Project Results) – WATERLOO BIOFILTER. (1995). *Trickling Filters - General*.

Ntuli, F., Omoregbe, I., Kuipa, P., Muzenda, E. and Belaid, M. (2009). *Characterization of Effluent from Textile Wet Finishing Operations. WCECS,* 1: 20-22.

Nur farhana jaafar, Aisha, A.J., Muh'd N.M.M., Norzahir, S., Azrul, H.S. (2012).*Daylight Photocatalysis by Carbon-Modified Titanium Dioxide, Angewandte Chemie International Edition,* 42: 4908-4911.

Pardeshi, S.K. and Pawar, R.Y. (2011).*$SrFe_2O_4$ complex oxide an effective and environmentally benign catalyst for selective oxidation of styrene*, Journal of Molecular Catalyst. *A,* 334: 35–43.

Pelaez, M., de la Cruz, A.A., O'Shea, K., Falaras, P. and Dionysiou, D.D. *(*2011).*Effects of water parameters on the degradation of microcystin-LR under visible light-activated TiO2 photocatalyst.*Journal of Water Resource, *45*: 3787–3796.

Pelentridou, K., Stathatos, E., Karasali, H. and Lianos, P. *(*2009).*Photodegradation of the herbicide azimsulfuron using nanocrystalline titania films as photocatalyst and low intensity black light radiation or simulated solar radiation as excitation source.* Journal of Hazardous Materials, 163: 756–760.

Peralta-Hernández, J.M., Manríquez, J., Meas-Vong, Y., Rodríguez, F.J., Chapman, T.W., Maldonado, M.I. and Godínez, L.A. (2007).*Photocatalytic properties of nano-structured TiO_2-carbon films obtained by means of electrophoretic deposition.* Journal of Hazardous Materials,147: 588-593.

Ping, C. Wei, L., Tianle, Z., Yanping, J. and Mingyuan, G. (2014).*Physical and Photocatalytic properties of $ZnFe_2O_4/TiO_2$ under visible light irradiation.*Journal of photochemistry and Photobiology, 168: 97-101.

Prithviraj, S., Park, Y., Kim, W., Park, H., Tachikawa, T. Majima, T., Choi,W. (2000). *Zinc ferrite -doped TiO_2 photocatalyst synthesized without using an external carbon precursor and the visible light activity.Journal of Applied Catalysis.* B 91: 355–361

Qiu, J., Wang, C. and Gu, M. (2004). *Photocatalytic properties and optical absorption of zinc ferrite nanometer films.*Journal of Material Science Engineering.B, 112: 1–4.

Rincon A.-G. and Pulgarin, C. (2005). *Use of coaxial photocatalytic reactor (CAPHORE) in the TiO_2 photo-assisted treatment of mixed E. coli and Bacillus sp. and bacterial community present in wastewater.* Journal of Catalysis, 101: 331–344.

Rockafellow, E.M.; Stewart, L.K. and Jenks, W.S. *(*2009).*Is sulfur-doped TiO_2 an effective visible light photocatalyst for remediation?* Journal of Applied Catalyst.B,91: 554–562.

Rong, S., Lin, S., Lanqin, T. and Zhidong, C. (2012). *Preparation and Characterization of magnetic core-shell $ZnFe_2O_4$ @ ZnO nanoparticles and their application for the Photodegradation of Methylene Blue.*Journal of Chemical Engineering,217: 185-191.

Rosales Bento Serrano., Lasa, de I. Hugo, Aaron Ortiz and Miguel Salaices.(2007). *Quasi equilibrium adsorption in heterogeneous photocatalyst.*Journal of Chem. Eng. Sci. 62: 5160 – 5166.

Sears, G. W. (1981). *Determination of specific surface area by titration with sodium hydroxide*.Journal of Analytical chemistry 28.

Sesha, S., Srini, V., Jeremy, W. and Elias S.K. (2006).*Synthesis and Characterization of Photocatalytic TiO_2 - $ZnFe_2O_4$ nanoparticles.*Journal of Nanomaterials, 2006: 1-4.

Sirtori, C., Zapata, A., Malato, S., Gernjak, W., Fernandez-Alba, A.R. and Aguera, A. *(*2009).*Solar photocatalytic treatment of quinolones: Intermediates and toxicity evaluation.*Journal of Photochemical, photobiological science, *8*: 644–651.

Sonal, S., Rimi, S. Charnji, S. and Bansal, S. (2013). *Enhanced Photocatalytic degradation of Methylene Blue using $ZnFe_2O_4$/MWCNT composite synthesized by hydrothermal method.* Journal of Material science,2013: 6.

Sue, K., Aoki, M., Sato, T., Nishio-Hamane, D., Kawasaki, S., Hakuta, Y., Takebayashi, Y., Yoda, S., Furuya, T., Sato, T. and Hiaki, T. (2011). *Continuous hydrothermal synthesis of nickel ferrite nanoparticles using a central collision-type micromixer: effects of temperature, residence time, metal salt molality, and NaOH addition on conversion, particle size, and crystal phase, Ind.* Journal of Engineering and Chemical Resources, 50: 9625–9631.

Tian, G., Fu, H., Jing, L. and Tian, C. (2009).*Synthesis and photocatalytic activity of stable nanocrystalline TiO_2 with high crystallinity and large surface area.*Journal of Hazardous Materials. 161: 1122-1130.

Tripathy T, De B (2006) *Flocculation: A New Way to Treat the Waste Water.* Journal of Physical Science,10: 93-127.

Tsukada, M., Abe, K., Yonemochi, Y., Ameyama, A., Kamiya, H. and Kambara, S. (2008). *Powder Technol.,* 180: 232.

Vautier, M., Guillard, C. and Herrmann, J. (2001).*Photocatalytic degradation of dyes in water: Case study of Indigo and of Indigo Carmine.* Journal of catalysis. 201: 46-59.

Venkatachalam, N., Palanichamy, M. and Murugesan, V. (2007).*Sol–gel preparation and characterization of alkaline earth metal doped nano TiO_2 Efficient photocatalytic degradation of 4-chlorophenol.*Journal of Molecular Catalysis. A Chemical, 273: 177–185.

Von Gunten, U. and Hoigne, J. (1994).*Bromate Formation during Ozonization of Bromide-Containing Waters: Interaction of Ozone and Hydroxyl Radical Reactions.* Journal of Environmental Science & Technology, 28: 1234.

Wang, C., Zhang, X., Liu, H., Li, X., Li, W. and Xu, H. *(*2009).*Reaction kinetics of photocatalytic degradation of sulfosalicylic acid using TiO_2 microspheres.*Journal of Hazardous Materials, *163*: 1101–1106.

Wang, C., Sun, L., Yun, H., Li, J., Lai, Y. and Lin, C. *(*2012).*Sonoelectrochemical synthesis of highly photoelectrochemically active TiO_2 nanotubes by incorporating cds nanoparticles.*Journal of Nanotechnology,20: 295-601.

Wiklund, L., Basu, S. and Miclescu, A. (2007). *Neuro- and cardioprotective effects of blockade of nitric oxide action by administration of methylene blue.*Journal of Academic Science, 1122: 231-244.

Wainwright, M., Crossley K.B. (2013).*Anaerobic sludge digestion, part II.Preparations, photocatalytic properties of magnetically separable nitrogen-doped TiO_2 supported on nickel ferrite.* Journal of Applied Catalyst.*B,* 71: 177–184.

WTS (Water Treatment Solutions). (2012) *Phorate degradation by TiO_2 photocatalysis: parameter and reaction pathway investigations.*Journal of desalination, 10: 1016 – 3026.

WWS (Waste Water System).(2013). *Ion exchange application in wastewater Treatment.*Journal of environmental biology,125: 311-323.

Xu, S., Shangguan, W., Yuan, J., Shi, J. and Chen, M. (2007).*Preparations and photocatalytic degradation of methyl orange in water on magnetically separable Bi_{12} TiO_{20} supported on nickel ferrite, Sci. Technol.*Journal of Advance Materials, 8: 40–46.

Yang, Y., Jiang, Y., Wang, Y., Sun, Y., Liu, L. and Zhang, J. (2007).*Influences of sintering atmosphere on the formation and photocatalytic property of $BaFe_2O_4$.*Journalof Mater. Chem. Phys., 105: 154–156.

Yasui, H., Nakamura, K., Sakuma, S., Iwasaki, M. and Sakai, Y. (1996). *A Full-Scale Operation of a Novel Activated Sludge Process without Excess Sludge Production.*Journal of Water Science and Technology 34: 395-404.

Yogo K. and Ishikawa, M. (2000).*Recent progress in environmental catalytic technology,"* Journal of Catalysis Surveys from Japan, 4: 83–90.

Yusuff, R. and Sonibare, J. (2004*). Characterization of Textile Industries 'Effluents in Kaduna, Nigeria and Pollution Implications, Global nest:* Indian Journal. 6: 212-221.

Zhang, B., Zhang, J. and Chen, F. (2008).*Preparation and characterization of magnetic $TiO_2/ZnFe_2O_4$ photocatalysts by a sol–gel method.*Journal of Res. Chemical Intermediate, 34: 375–380.

Zhang, L., Zhou, X., Guo, X., Song, X. and Liu, X. (2011).*Investigation on the degradation of acid fuchsin induced oxidation by $MgFe_2O_4$ under microwave irradiation.* Journal of Molecular Catalyst. A, 335 31–37.

Zhen, L., Jiayi, S., Yan, W., Yiming, X. (2013). *Enhanced Photocatalytic activity and stability of alumina supported hematite for azo dye degradation in aerated aqueous suspension.* Journal of Hazardous materials,254-255: 18-25.

Zhu, Z., Li, X., Zhao, Q., Li, H., Shen, Y. and Chen, G. (2010). *Porous ''Brick-Like'' $NiFe_2O_4$ nanocrystals loaded with ag species towards effective degradation of toluene.* Journal of Chemical Engineering,Amsterdam, Netherland, 165: 64–70.

Zhou, H. and Smith, D.W. (2002).*Advanced technologies in water and wastewater treatment.*Journal of Environmental Engineering and Science, 1: 247-264.

APPENDIX A

Material balance

$ZnCl_2 + 2FeCl_2 + 8NaOH \rightarrow Zn(OH)_2 + 2Fe(OH)_3 + 8NaCl$ **(1)**

mm 127 172 40

$Zn(OH)_2 + 2Fe(OH)_3 \rightarrow ZnFe_2O_4 + 4H_2O$

To produce 100g of $ZnFe_2O_4$

M.W of $ZnFe_2O_4$ = 251 g/mol

Mole of $ZnFe_2O_4$ = 100/251 = 0.4 mol

$Zn(OH)_2 + 2Fe(OH)_3 \rightarrow ZnFe_2O_4 + 4H_2O$

0.4 mol 0.8 mol 0.4 mol

Therefore, to produce 0.4 mol of $ZnFe_2O_4$

The amount of NaOH and $FeCl_3$ required.

$FeCl_3 + 3NaOH \rightarrow Fe(OH)_3 + 3NaCl$

1 3 1 3

0.8 mol 3*0.8 =2.4 mol 0.8 mol

138 g 96 g

$ZnCl_2 + 2NaOH \rightarrow Zn(OH_2) + 2NaCl_2$ (2)

1 2 1 1

0.4 mol 2*0.4 mol

51 g 32 g.

$ZnCl_2$ = 51 g

$FeCl_3$ = 138 g

NaOH = 96 + 32 = 128 g

Down size the required amount into 2

Given

$ZnCl_2$ = 25.5 g

$FeCl_3$ = 69 g

NaOH = 70 g

APPENDIX B

CRYSTALLITE SIZE ANALYSIS USING XRD

1. 10 wt% $ZnFe_2O_4/\alpha\text{-}Al_2O_3$

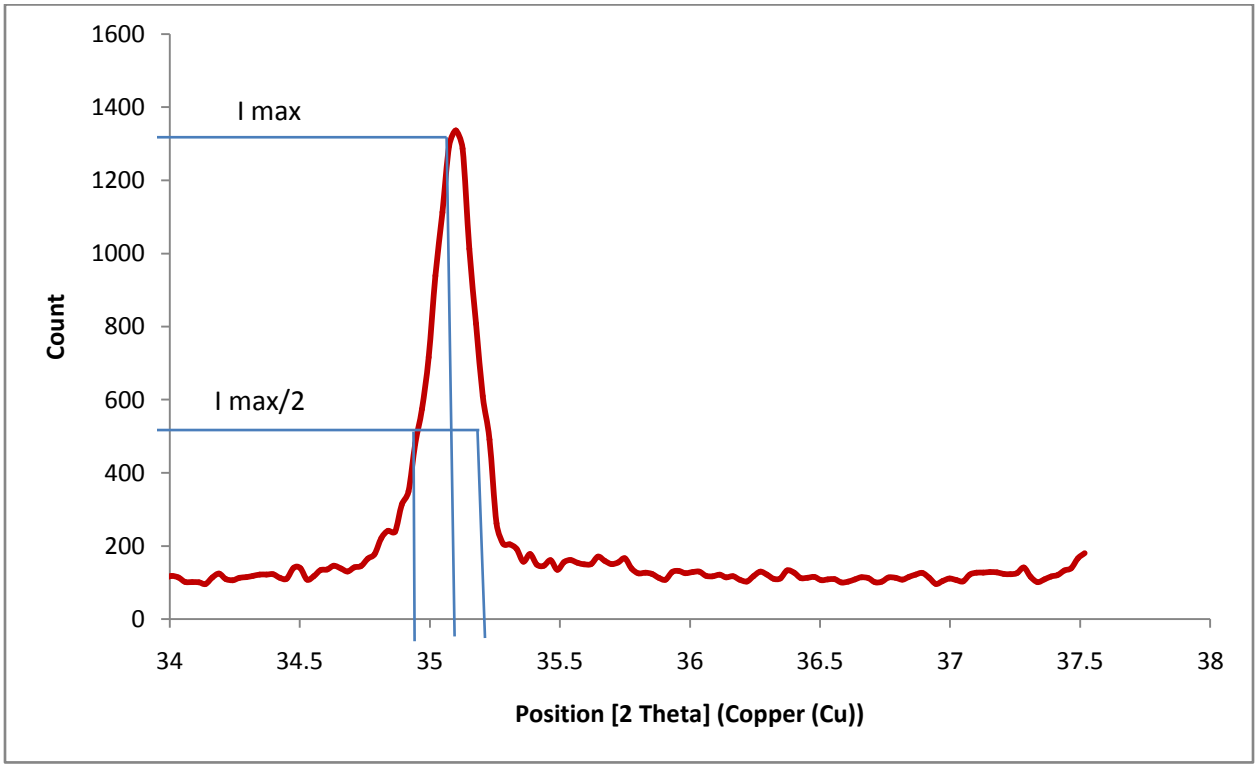


Fig. B1. XRD showing the peaks for evaluating β and θfor 10 wt% $ZnFe_2O_4/\alpha\text{-}Al_2O_3$ composite photocatalyst.

Using Scherrer's equation

$$D = \frac{0.9\lambda}{\beta cos\theta}$$

Where, D = Particle size, nm.

λ = 1.54 Å

B = Width at Full Width at Half Maximum (FWHM) in radians.

2θ = Bragg angle.

$\Theta_1 = 57.30$

$\Theta_2 = 57.65$

$2\Theta = 57.43^0 \quad \Theta = 28.72$

$$D = \frac{0.9\lambda}{\beta cos\theta} = \frac{0.94*0.1542}{0.00611*\cos(28.72)} = 27.1\ nm$$

2. 20 wt% $ZnFe_2O_4/\alpha\text{-}Al_2O_3$

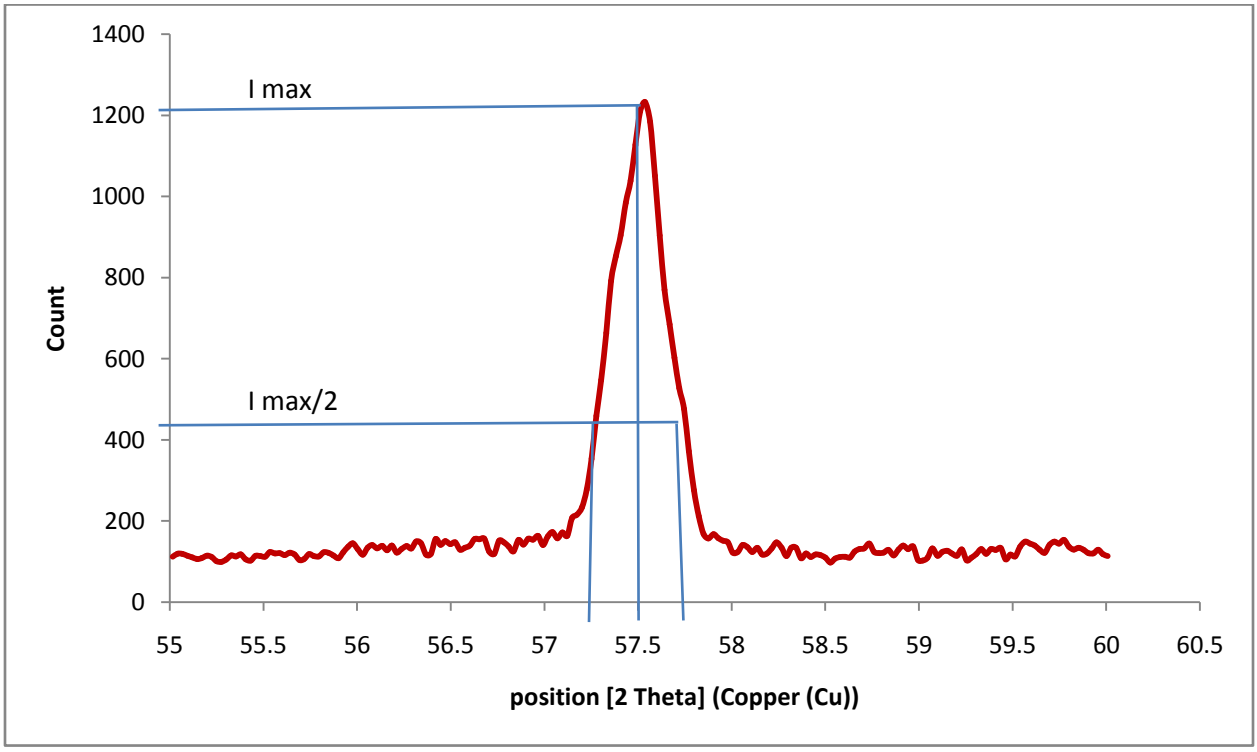


Fig. B2. XRD showing the peaks for evaluating β and θfor 20 wt% $ZnFe_2O_4/\alpha\text{-}Al_2O_3$ composite photocatalyst.

$\Theta_1 = 57.35$

$\Theta_2 = 57.65$

$2\Theta = 57.54^0 \quad \Theta = 28.77$

$$D = \frac{0.9\lambda}{\beta cos\theta} = \frac{0.94*0.1542}{0.00524*\cos(28.77)} = 31.56\ nm$$

3. 30 wt% $ZnFe_2O_4/\alpha\text{-}Al_2O_3$

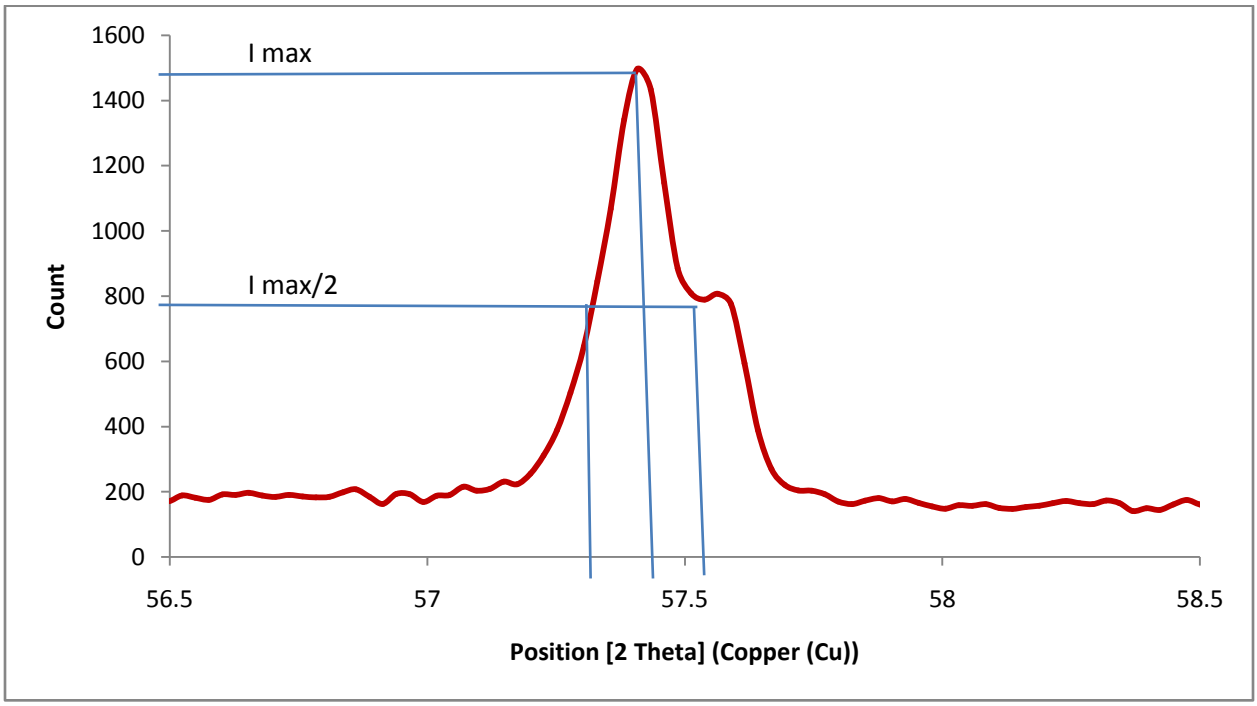


Fig. B3. XRD showing the peaks for evaluating β and θfor 30 wt% $ZnFe_2O_4/\alpha\text{-}Al_2O_3$ composite photocatalyst.

$\Theta_1 = 57.32$

$\Theta_2 = 57.48$

$2\Theta = 57.42^0 \quad \Theta = 28.71$

$$D = \frac{0.9\lambda}{\beta cos\theta} = \frac{0.94*0.1542}{0.00279*\cos(28.71)} = 59.23\ nm$$

4. 40 wt% $ZnFe_2O_4/\alpha\text{-}Al_2O_3$

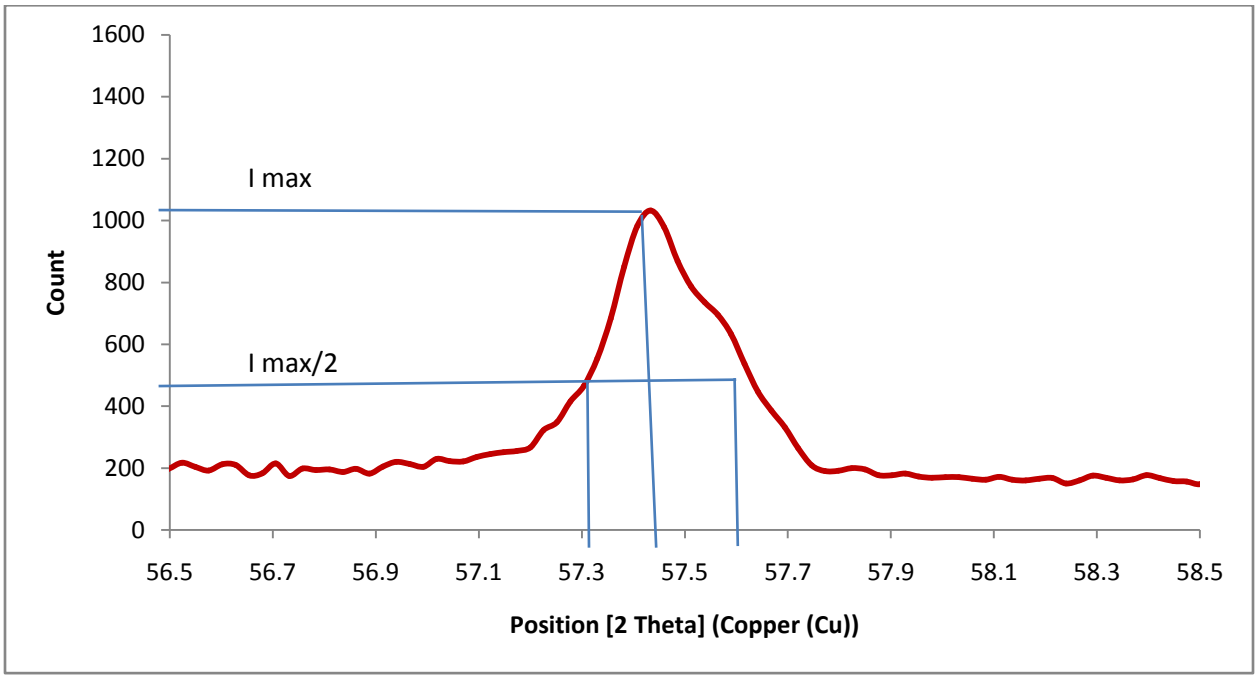


Fig. B4. XRD showing the peaks for evaluating β and θfor 40 wt% $ZnFe_2O_4/\alpha\text{-}Al_2O_3$ composite photocatalyst.

$\Theta_1 = 57.37$

$\Theta_2 = 57.90$

$2\Theta = 57.44^0 \quad \Theta = 28.72$

$$D = \frac{0.9\lambda}{\beta cos\theta} = \frac{0.94*0.1542}{0.00925*\cos(28.72)} = 75.2\ nm$$

APPENDIX C

SURFACE AREA DETERMINATION

$$s\left(\frac{m^2}{g}\right) = 32V - 25$$

$ZnFe_2O_4$

$$Specific\ surface\ area = 32V - 25$$

$$= 32 * 11.6 - 25 = 397.4\ m2/g$$

10 wt% $ZnFe_2O_4/Al_2O_3$

$$Specific\ surface\ area = 32V - 25$$

$$= 32 * 7.6 - 25 = 269.4\ m2/g$$

20 wt% $ZnFe_2O_4/Al_2O_3$

$$Specific\ surface\ area = 32V - 25$$

$$= 32 * 4.9 - 25 = 183\ m2/g$$

30 wt% $ZnFe_2O_4/Al_2O_3$

$$Specific\ surface\ area = 32V - 25$$

$$= 32 * 1.7 - 25 = 80.6\ m2/g$$

APPENDIX D

DETERMINATION OF POINT OF ZERO CHARGE OF THE SYNTHESIZED CATALYSTS

Table D. Determination of pH of Zero point of charge

pH initia	$ZnFe_2O_4$	10 wt% $ZnFe_2O_4/Al_2O_3$	20 wt% $ZnFe_2O_4/Al_2O_3$	30 wt% $ZnFe_2O_4/Al_2O_3$
	pH final			
2	2.42	2.47	2.07	1.96
3	7.08	6.74	3.20	3.31
4	7.69	4.25	4.01	8.06
5	7.85	7.62	7.49	9.90
6	9.10	8.15	8.02	6.73
7	8.02	9.78	7.78	8.15
8	7.97	6.67	8.01	8.47
9	8.06	7.85	8.49	7.97
10	9.26	8.82	8.75	9.44
11	10.59	10.19	10.06	10.62
12	11.88	11.81	11.66	11.94

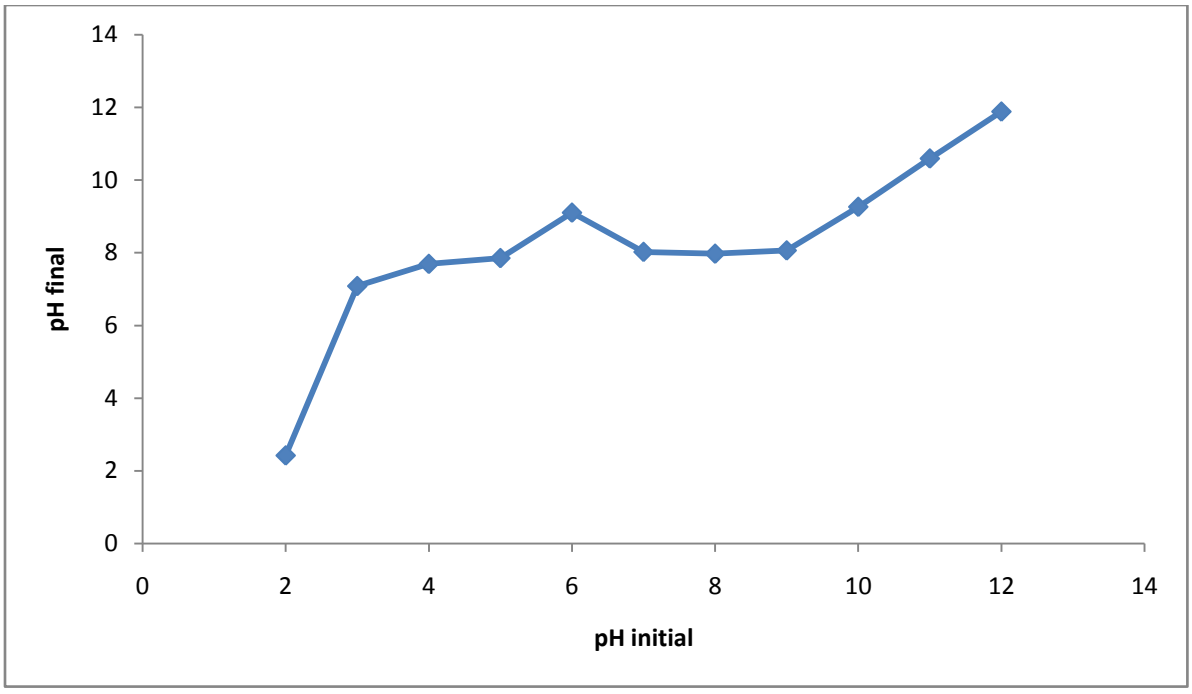


Fig. D1. PZC determination of the synthesized $ZnFe_2O_4$

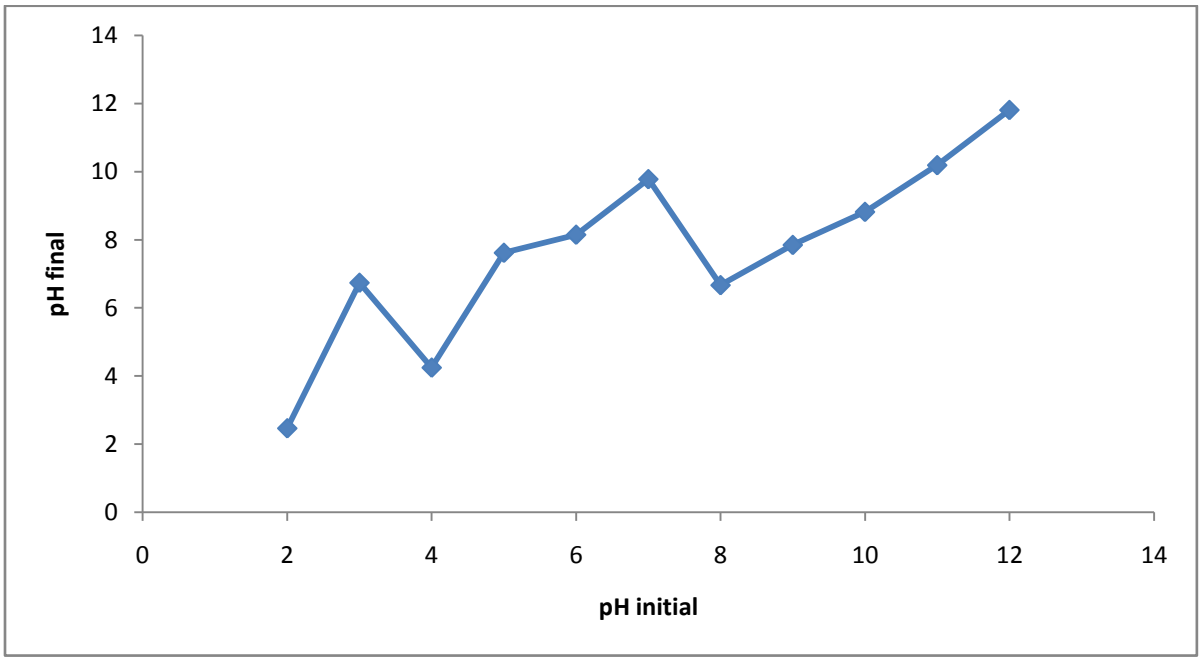


Fig. D2. PZC determination of the synthesized 10 wt% $ZnFe_2O_4/\alpha\text{-}Al_2O_3$

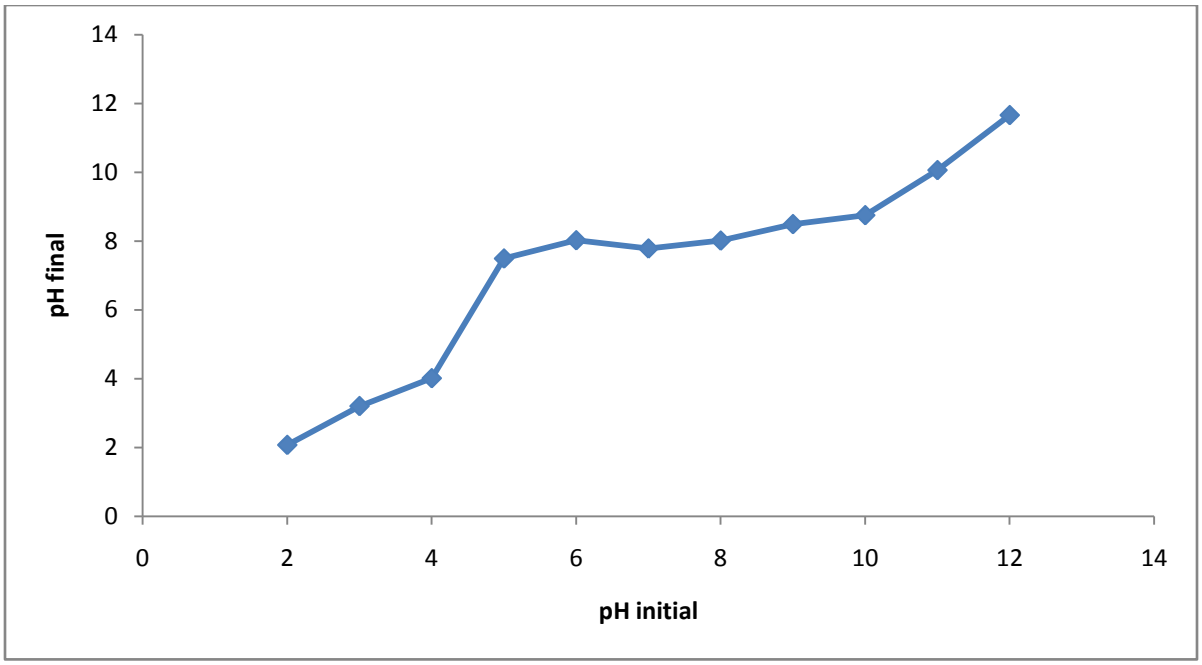


Fig. D3. PZC determination of the synthesized 20 wt% $ZnFe_2O_4/\alpha\text{-}Al_2O_3$

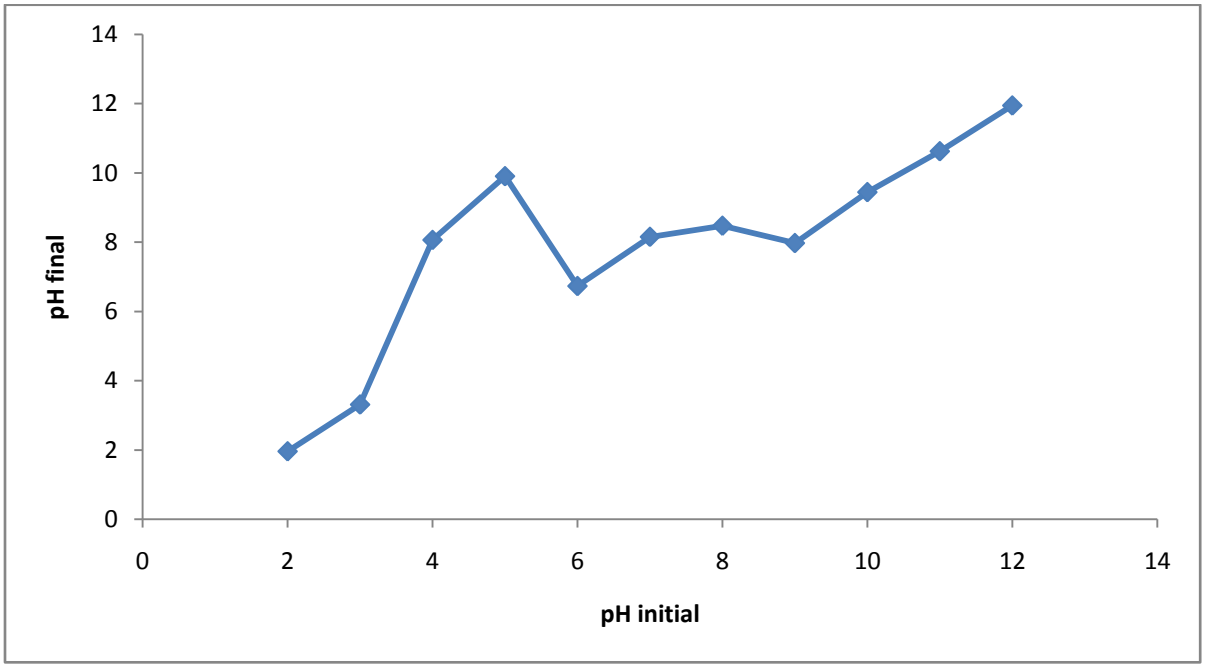


Fig. D4. PZC determination of the synthesized 30 wt% $ZnFe_2O_4/\alpha\text{-}Al_2O_3$

APPENDIX E

UV-vis ANALYSIS OF DECOLOURIZED MB SOLUTION

Table E. UV-Vis Absorption spectra of decolourized MB solution with time under photocatalysis.

Photocatalyst	**$ZnFe_2O_4$**		**10 wt% $ZnFe_2O_4$/α-Al_2O_3**		**20 wt% $ZnFe_2O_4$/α-Al_2O_3**		***30 wt% $ZnFe_2O_4$/α-Al_2O_3***		**40 wt% $ZnFe_2O_4$/α-Al_2O_3**	
	Concentrations									
Time (min)	**100**	**25**	**100**	**25**	**100**	**25**	**100**	**25**	**100**	**25**
0	1.891	0.486	1.899	0.410	1.912	0.356	1.020	0.385	1.012	0.322
5	0.707	0.263	0.947	0.314	0.852	0.242	0.743	0.225	0.859	0.199
10	0.600	0.227	0.932	0.238	0.821	0.228	0.719	0.204	0.812	0.195
15	0.560	0.219	0.917	0.211	0.797	0.219	0.681	0.176	0.790	0.177
20	0.507	0.205	0.897	0.198	0.677	0.180	0.663	0.146	0.774	0.175
30	0.501	0.196	0.872	0.175	0.658	0.167	0.647	0.124	0.756	0.164
40	0.497	0.157	0.854	0.138	0.643	0.148	0.628	0.115	0.723	0.145
50	0.469	0.560	0.846	0.127	0.622	0.117	0.603	0.100	0.688	0.136
60	0.429	0.143	0.765	0.116	0.587	0.098	0.589	0.088	0.653	0.129
90	0.412	0.120	0.753	0.105	0.573	0.088	0.576	0.073	0.611	0.121

APPENDIX F

DETERMINATION OF COD OF DEGRADED MB SOLUTION

COD Determination of degraded of MB solution under photocatalysis.

$$COD = \frac{V_b * V_t * M * 16000}{Volume\ of\ sample\ used}$$

Where, V_t = Titered volume

V_b = Volume of the blank sample

M = Concentration of sample

Using $ZnFe_2O_4$

V_b = 18.4

V_t = 14.6

M = 0.05

COD = 18.4 – 14.6*0.05*16000/5 = 608

Using 20 wt% $ZnFe_2O_4/Al_2O_3$

COD = 18.4 – 13.5*0.05*16000/5 = 784

COD Determination of degraded of Textile effluent under photocatalysis

Using $ZnFe_2O_4$

COD = 9.1 – 5.5*0.05*16000/5 = 576

Using 20 wt% $ZnFe_2O_4/Al_2O_3$

COD = 9.1 – 6.5*0.05*16000/5 = 416